

## Formation of superheavy elements in cold fusion reactions

V. Yu. Denisov<sup>1,2,\*</sup> and S. Hofmann<sup>1,†</sup>

<sup>1</sup>GSI-Darmstadt, Planckstrasse 1, D-64220 Darmstadt, Germany

<sup>2</sup>Institute for Nuclear Research, Prospect Nauki 47, 252028 Kiev, Ukraine<sup>‡</sup>

(Received 10 February 1999; revised manuscript received 17 August 1999; published 14 February 2000)

The process of the synthesis of *superheavy elements* (SHEs) is not yet understood completely. In the presented work we make an attempt to describe the cold fusion reactions of the type  $X + (\text{Pb,Bi}) \rightarrow \text{SHE} + 1n$  at subbarrier energies. The process of the formation of SHEs is subdivided into three steps. (1) The capture of two spherical nuclei and the formation of a common shape of the two touching nuclei. Low-energy surface vibrations and transfer of few nucleons are taken into account in the first step of the reaction. (2) The formation of a spherical or near spherical compound nucleus. (3) The survival of the excited compound nucleus due to evaporation of neutrons and  $\gamma$ -ray emission in competition with fission. A lowering of the fission barrier was taken into account, which arises from a reduction of shell effects at increasing excitation energy of the compound nucleus. The following reactions were analyzed in detail:  $(^{58}\text{Fe}, ^{64}\text{Ni}, ^{70}\text{Zn}, ^{78}\text{Ge}) + ^{207}\text{Pb}$ ,  $(^{50}\text{Ti}, ^{54}\text{Cr}, ^{58}\text{Fe}, ^{59}\text{Co}, ^{62,64}\text{Ni}, ^{65}\text{Cu}, ^{66,68,70}\text{Zn}, ^{71}\text{Ga}, ^{74,76,78}\text{Ge}, ^{75}\text{As}, ^{80,82}\text{Se}) + ^{208}\text{Pb}$ ,  $(^{58}\text{Fe}, ^{64}\text{Ni}, ^{70}\text{Zn}, ^{78}\text{Ge}) + ^{210}\text{Pb}$ , and  $(^{50}\text{Ti}, ^{54}\text{Cr}, ^{58}\text{Fe}, ^{64}\text{Ni}, ^{70}\text{Zn}, ^{78}\text{Ge}) + ^{209}\text{Bi}$ . The presented model describes well the available experimental cross-section data and allows for predicting cross-section values for the synthesis of so-far unknown heavier elements.

PACS number(s): 25.60.Je, 25.60.Pj, 25.70.Hi, 25.70.Jj

### I. INTRODUCTION

The synthesis of superheavy elements (SHEs) was and still is an outstanding research object. The properties of SHEs were studied both theoretically as well as experimentally [1–27]. In two series of experiments the heaviest elements from 107 to 109 and from 110 to 112 were synthesized at GSI in Darmstadt by using cold fusion [1,2]. In cold fusion, SHEs are synthesized by reactions of the type  $X + (\text{Pb,Bi}) \rightarrow \text{SHE} + 1n$  at subbarrier energies. The excitation energy of a compound nucleus formed by cold fusion is low, approximately 10–20 MeV only. It was measured that the kinetic energy of the reaction partners in the center-of-mass system corresponds to the fusion barrier or is even less [2]. The cross section for the synthesis of SHEs is very small and decreases strongly with increasing atomic number.

The fission barrier of SHEs is determined by the shell structure [8,9,16–26], because the contribution of the macroscopic liquid-drop part to the fission barrier is close to zero or, for the heaviest systems, even negative. A method to include shell-structure effects in calculations at large nuclear deformation, so for heavy-element fission barriers, was introduced successfully by Strutinsky [8].

The properties of SHEs were investigated theoretically using the Strutinsky method [8,9,16–26]. The ground-state deformation, the fission barrier, the binding energy and the competition between various possible decay modes was studied [16–20]. However, the dynamical process leading to the formation of SHEs by heavy-ion fusion reactions is not yet understood well enough. Only recently, few attempts were undertaken to develop models for describing the fusion pro-

cess and for reproducing the measured cross-section data [14–18].

The concept of a dynamically developing dinuclear system was used in [12,13] in order to estimate cold-fusion reaction cross sections. As a fitting parameter the survival probability of the compound nucleus was adjusted, and the cross sections measured at the maximum of the excitation function could be reproduced. However, the energy dependence of the cross section and the shape evolution of the dinuclear system were not considered.

The dynamical models discussed in [14,15] for describing the fusion are based on diffusion processes forming SHEs. Starting from the shape of two touching nuclei the configuration evolves to a near spherical compound-nucleus shape. The models were applied for the evaluation of cross-sections forming SHEs in fusion reactions at energies well above the barrier. In this hot fusion reaction the compound nucleus cools down by evaporation of several neutrons. Hot fusion was recently used in Dubna for an experimental investigation of elements up to 114 [3,5].

The measured excitation functions for the formation of SHEs by cold fusion reveal a narrow width of the curves and a shift of the position to smaller excitation energies with increasing element number [2,6]. An appropriate model should reproduce also these observed phenomena. In the following we present a model aiming at reproducing the measured excitation functions for the synthesis of SHEs.

Because the cold fusion is observed at energies below the barrier, we consider as a first step in the model the capture process and the penetration of the fusion barrier (Sec. II).

The formation of a compound nucleus of a near spherical equilibrium shape occurs after capture. A barrier develops on the way from the touching configuration of two spherical nuclei to the near spherical compound-nucleus shape. The shape evolution and the transmission through the barrier on

\*Electronic address: denisov@gsi.de, denisov@kinr.kiev.ua

†Electronic address: s.hofmann@gsi.de

‡Permanent address.

the way to the spherical or near spherical configuration are discussed in Sec. III. The last step of the reaction is determined by the evaporation of nucleons and the emission of  $\gamma$  quanta forming SHEs in the ground state. These processes are in competition with fission (Sec. IV).

In Sec. V, the obtained results are discussed and compared with the available experimental data. The conclusion is presented in Sec. VI.

## II. TRANSMISSION THROUGH THE FUSION BARRIER

Various mechanisms were discussed to explain the phenomenon of subbarrier fusion: the excitation of low energy states in projectile and target nucleus [28–32], the transfer of nucleons [28,29,32–35], the barrier reduction due to deformed nuclear shapes and the neck formation [36]. It was shown that the fusion cross section is strongly enhanced by the coupling to both the low-energy surface vibrations [28–32] and the few-nucleon transfer channels [32–35].

The model which we apply here for the barrier penetration is discussed in more detail in [33]. In the following, we present the main features of the model. It describes well the experimental data of the fusion cross sections  $\sigma_{\text{fus}}(E)$  as well as of the mean angular momenta  $\langle L(E) \rangle$  in the case of lighter nuclei. The enhancement of subbarrier penetration due to the coupling to both the low-energy surface excitations and the neutron transfer is taken into account.

### A. Barrier transmission enhanced by low-energy surface vibrations

The system of coupled channel equations in the case of coupling to the low-energy vibrational states has the form [28–32]

$$\left[ -\frac{\hbar^2}{2\mu_i} \frac{d^2}{dr^2} + \frac{\hbar^2 l_i(l_i+1)}{2\mu_i r^2} + V(r) - Q_i - E \right] \varphi_i(r) = -\sum_j V_{ij}(r) \varphi_j(r), \quad (1)$$

where  $\psi_i(r) = \varphi_i(r)/r$  is the wave function,  $\mu_i$  is the reduced mass,  $l_i$  is the value of the orbital angular momentum in units of  $\hbar$ ,  $V(r)$  is the nucleus-nucleus interaction potential,  $Q_i$  is the  $Q$  value of the reaction in channel  $i$ ,  $E$  is the collision energy, and  $V_{ij}(r)$  is the coupling potential. The coupling potential between the ground-state and the channels connected with the low-energy surface vibrational state of multipolarity  $\lambda$  is given by [28,29,31–33]

$$V_{0i} = \frac{\beta_i R_i}{\sqrt{4\pi}} \left[ \frac{dV_{i-1}(r)}{dr} + \frac{3}{2\lambda+1} \frac{z_1 z_2 e^2 R_i^{\lambda-1}}{r^{\lambda+1}} \right]. \quad (2)$$

Here  $V_{i-1}(r)$  is the nuclear part of the interaction potential  $V(r)$ ,  $z_1$  and  $z_2$  are the proton numbers,  $e$  is the charge unit, and  $\beta_i R_i$  is the deformation length of the  $i$ th vibrational state in the nucleus with radius  $R_i$ .

As in [31–33], we assume that all reduced masses  $\mu_i$  and orbital angular momenta  $l_i$  are equal in all channels related to

the vibrational excitations. Then, by setting the radial dependence of the coupling potential at the barrier position  $V_{ij}(r) = V_{ij}(\bar{R})$ , we diagonalize the system (1) with the help of the substitution

$$\varphi_i(r) = \sum_k U_{ik} \xi_k(r), \quad (3)$$

where  $U_{ik}$  is the transformation matrix and  $\xi_k(r)$  is the wave function (eigenvector). The coupling matrix  $\mathcal{M}_{ij}$  takes the form

$$\sum_{ij} U_{ki} \mathcal{M}_{ij} U_{jl} = \sum_{ij} U_{ki} [-Q_i \delta_{ij} + V_{ij}(\bar{R})] U_{jl} = \epsilon_k \delta_{kl} \quad (4)$$

and after diagonalization we find the eigenvalue  $\epsilon_k$ . In this case the partial fusion cross section  $\sigma(E, l)$  is equal to [29,31,32]

$$\sigma(E, l) = \frac{\pi \hbar^2}{2\mu E} (2l+1) \sum_k |U_{k0}|^2 T(E, \mathcal{V}_{lk}), \quad (5)$$

where  $T(E, \mathcal{V}_{lk})$  is the transmission coefficient obtained for the one-dimensional effective potential  $\mathcal{V}_{lk}$

$$\mathcal{V}_{lk}(r) = V_l(r) + \epsilon_k = V(r) + \hbar^2 l(l+1)/(2\mu r^2) + \epsilon_k. \quad (6)$$

We conclude from Eq. (5) that the partial cross section for fixed  $E$  and  $l$  is determined by the sum of the transmission coefficients  $T(E, \mathcal{V}_{lk})$  obtained for the effective potential  $\mathcal{V}_{lk}$  with the weights  $|U_{k0}|^2$ . The effect of fusion cross-section enhancement due to the coupling to the low-energy vibrational states is related to the smallest eigenvalue  $\epsilon_k$ , which is negative and lowers the interaction potential.

The total fusion cross section is equal to

$$\sigma_{\text{fus}}(E) = \sum_l \sigma(E, l). \quad (7)$$

The total fusion cross section is identical to the capture cross section, the first step in the formation process for SHEs.

### B. Barrier transmission enhanced by nucleon transfer

Let us consider the transfer reaction in the DWBA approach, which describes well the nucleon-transfer reactions near and below the barrier [28]. In the DWBA approximation we neglect the influence of the transfer channels on other reaction channels. In this case the matrix  $\mathcal{M}$  has a box structure. Each box of the matrix  $\mathcal{M}$  in Eq. (4) is similar to the respective box without transfer. For each transfer channel we have an enhancement described by Eqs. (4), (5), and (7). Because the energy and the deformation length of the vibrational states vary only little for nuclei, which differ by several nucleons, we assume that the values of  $\epsilon_k$  and  $|U_{k0}|^2$  for each specific transfer channel do not differ much from the ones obtained in Eq. (4) without transfer. In this case the partial fusion cross section of the transfer channel  $f$  is deter-

mined also by Eqs. (4)–(6), but the transmission coefficient should be calculated by taking into account the few-nucleon transfer.

If the energy of the collision is smaller than the barrier of the effective potentials before and after nucleon transfer and if the transfer occurs at the distance  $r_{tr}$ , then the transmission coefficient may be written as [33]

$$T(E, \mathcal{V}_{lk}^i, \mathcal{V}_{lk}^f) = 1/\{1 + \exp[\mathcal{A}(E, \mathcal{V}_{lk}^i, \mathcal{V}_{lk}^f, r_{tr})]\}, \quad (8)$$

where the action  $\mathcal{A}(E, \mathcal{V}_{lk}^i, \mathcal{V}_{lk}^f, r_{tr})$  is given by

$$\begin{aligned} \mathcal{A}(E, \mathcal{V}_{lk}^i, \mathcal{V}_{lk}^f, r_{tr}) = & \mathcal{A}^i(E, \mathcal{V}_{lk}^i, r_{tr}) + \mathcal{A}^{tr}(E, r_{tr}) \\ & + \mathcal{A}^f(E, \mathcal{V}_{lk}^f, r_{tr}). \end{aligned} \quad (9)$$

We apply the Landau method for the integration over a complex classical paths in the case of transitions between systems with arbitrary degrees of freedom, see for details [33] and Eq. (52.1) and related text in [37,38]. The action

$$\mathcal{A}^i(E, \mathcal{V}_{lk}^i, r_{tr}) = (2/\hbar) \int_{r_{tr}}^{r_{lk}^i} \sqrt{2\mu_i(r)(\mathcal{V}_{lk}^i(r) - E)} dr, \quad (10)$$

describes the tunneling of ions in an effective potential before nucleon transfer  $\mathcal{V}_{lk}^i$  from the outer turning point  $r_{lk}^i$  up to  $r_{tr}$ , the action  $\mathcal{A}^f(E, \mathcal{V}_{lk}^f, r_{tr})$

$$\mathcal{A}^f(E, \mathcal{V}_{lk}^f, r_{tr}) = (2/\hbar) \int_{r_{lk}^f}^{r_{tr}} \sqrt{2\mu_f(r)(\mathcal{V}_{lk}^f(r) - E)} dr \quad (11)$$

is related to the tunneling of ions in an effective potential after nucleon transfer  $\mathcal{V}_{lk}^f$ ,

$$\mathcal{V}_{lk}^f(r) = V_{lk}^f(r) + \epsilon_k - Q_{tr}^f \quad (12)$$

from the point  $r_{tr}$  to the inner turning point  $r_{lk}^f$  of the effective potential  $\mathcal{V}_{lk}^f(r)$ . Here  $Q_{tr}^f$  is the  $Q$  value of the transfer reaction in channel  $f$ .

We assume that in the case of  $m$ -neutron transfer during barrier penetration in fusion of heavy ions the action  $\mathcal{A}^{tr}(E, r_{tr})$  connected with the nucleon transfer process can be written as

$$\mathcal{A}^{tr}(E, r_{tr}) = (2/\hbar) \sum_{i=1}^m \sqrt{2M\mathcal{E}_i(r_{tr} - R_{12} - \delta)}. \quad (13)$$

This form of the action describes the tunneling of  $m$  neutrons between square potential wells. In Eq. (13) we introduced a parameter  $\delta$ , which takes into account the finite diffuseness of a more realistic nucleon-nucleus potential. The barrier for the transferring nucleon disappears at the finite distance  $\delta$  between the surfaces of the reacting nuclei.

The wave function of the transferring nucleon may be concentrated more in the volume or more in the surface region of the parent nucleus. Therefore, the nucleon transfer amplitude, which is related to the overlap integral of the wave functions, can have its maximum at larger or smaller

distances of the colliding nuclei. This effect can be taken into account by a small variation of the parameter  $\delta$  in Eq. (13). We chose the same value  $\delta = 0.7$  fm as used in [33] for colliding systems at the  $\beta$ -stability line.

The distance  $r_{tr}$  at which the nucleon transfer takes place, is determined from the principle of minimal action, see Sec. 52 in [38]. Therefore, the integral over the tunnel trajectory including the few-nucleon transfer has its minimum value of the action (9) and its maximum value of the transmission coefficient (8). The few-nucleon transfer is especially important when  $Q_{tr}^f \gg 1$  MeV and the action (11) is small.

The action  $\mathcal{A}(E, \mathcal{V}_{lk}^i, \mathcal{V}_{lk}^f, r_{tr})$  is a function of the  $Q$  value of the transfer reaction and of the separation energy  $\mathcal{E}_i$  of the transferred nucleon. Therefore, the greatest enhancement of subbarrier fusion due to few-nucleon transfer happens at a small value of  $\mathcal{E}_i$  and at large positive  $Q$  value.

The expression (8) for the transmission coefficient is valid for collision energies  $E$  smaller than the effective barriers  $\bar{\mathcal{V}}_{lk}^i$  before, and  $\bar{\mathcal{V}}_{lk}^f$  after the few-nucleon transfer. In the case  $\bar{\mathcal{V}}_{lk}^f < E < \bar{\mathcal{V}}_{lk}^i$  and  $r_{tr} > \bar{R}_{lk}^f$ , the transmission coefficient has the form [33]

$$\begin{aligned} T(E, \mathcal{V}_{lk}^i, \mathcal{V}_{lk}^f) = & 1/\{1 + \exp[\mathcal{A}^i(E, \mathcal{V}_{lk}^i, r_{tr}) \\ & + \mathcal{A}^{tr}(E, r_{tr})]\} T_{HW}(E, \mathcal{V}_{lk}^f). \end{aligned} \quad (14)$$

Here  $\bar{R}_{lk}^f$  is the distance between ions at the barrier of the effective potential  $\mathcal{V}_{lk}^f$ ,  $T_{HW}(E, \mathcal{V}_{lk}^f)$  is the transmission coefficient for the effective barrier after transfer, obtained in the Hill-Wheeler approximation [39] and taking into account the reflection during barrier penetration. The subbarrier tunneling of nuclei before the nucleon transfer and the subbarrier nucleon transfer are described by the first term in Eq. (14). The term  $T_{HW}$  is related to reactions above the barrier after nucleon transfer.

If  $\bar{\mathcal{V}}_{lk}^f < E < \bar{\mathcal{V}}_{lk}^i$  and  $r_{tr} < \bar{R}_{lk}^f$ , then one should take into account the separation of the system after few-nucleon transfer. The transmission coefficient is written as [33]

$$\begin{aligned} T(E, \mathcal{V}_{lk}^i, \mathcal{V}_{lk}^f) = & 1/\{1 + \exp[\mathcal{A}^i(E, \mathcal{V}_{lk}^i, r_{tr}) + \mathcal{A}^{tr}(E, r_{tr})]\} \\ & \times (1 - T_{HW}(E, \mathcal{V}_{lk}^f)). \end{aligned} \quad (15)$$

We use the transmission coefficient in the Hill-Wheeler approximation at high collision energies  $E > \bar{\mathcal{V}}_{lk}^f$  and  $E > \bar{\mathcal{V}}_{lk}^i$ , however, do not take into account the enhancement of fusion due to nucleon transfer in this case. The expressions (14) and (15) are written for the case  $Q_{tr} > 0$  and may easily be transformed to the case  $Q_{tr} < 0$ .

The compound nucleus is formed after any kind of transfer. Therefore, the total capture cross section is the sum of Eq. (5) and of all possible transfer channels  $f$ , i.e.,

$$\begin{aligned} \sigma_{fus}(E) = & \frac{\pi \hbar^2}{2\mu E} \sum_l (2l+1) \sum_k |U_{k0}|^2 \left[ T(E, \mathcal{V}_{lk}^i) \right. \\ & \left. + \sum_f T(E, \mathcal{V}_{lk}^i, \mathcal{V}_{lk}^f) \right]. \end{aligned} \quad (16)$$

Note that the contributions to the total cross section are small for the channels with  $Q_{tr} \approx 0$  and are negligible for  $Q_{tr} \ll -1$  MeV due to the exponential dependence of the transmission coefficient.

Now, we determine the interaction potential between two nuclei at a distance  $r$ ,

$$V(r) = z_1 z_2 e^2 / r + V_{i-i}(r). \quad (17)$$

Various parametrizations of the nuclear part  $V_{i-i}(r)$  of the potential between spherical nuclei are known in literature [28,29,40]. We chose the Krappé-Nix-Sierk  $V_{KNS}(r)$  [40] potential in our calculation for  $r \geq R_{12} = R_1 + R_2$ . In order to avoid shape dependence for distances  $r < R_{12}$ , we use a parametrization of the interaction potential  $V(r)$  for  $r < R_{12}$  of the form

$$V_{fus}(r) = -Q_{fus} + x^2(c_1 + c_2 \exp(x)), \quad (18)$$

where  $Q_{fus}$  is the  $Q$  value of the fusion reaction calculated from the experimental masses [41] or the theoretical mass predictions [42,43]. The parameter  $x$  in the second term is only  $r$  dependent,  $x = (r - R_{fus}) / (R_{12} - R_{fus})$ ,  $R_{fus}$  is the distance between the centers of gravity of the left and right hemisphere of the compound nucleus. The coefficients  $c_1$  and  $c_2$  are obtained from equating the potentials  $V(r)$  (17) and  $V_{fus}(r)$  (18) and their derivatives at the touching point  $R_{12} = R_1 + R_2$ . We take a quadratic dependence of  $V_{fus}(r)$  at  $x = 0$ , because the potential (deformation) energy of the highly excited compound nucleus is minimum for a spherical shape, i.e., at  $x = 0$ . In our model the parametrization (18) is only needed close to distances  $R_{12}$ .

The reduced mass  $\mu$  for  $r > R_{12}$  is given by a standard expression, see for example [28]. The reduced mass in Eqs. (10) and (11) for  $r < R_{12}$  is a function of  $r$ . We used the parametrization of  $\mu(r)$  introduced in [25]

$$\mu_{i(f)}(r) = \mu_{i(f)} \left\{ (17/15)k \left[ (R_{12} - r) / (R_{12} - R_{fus}) \right]^2 \times \exp[-(32/17)(r/R_{fus} - 1)] + 1 \right\}, \quad (19)$$

with  $k = 16$ . This semiempirical dependence of the reduced mass was successfully used in calculations of the fission lifetime of heavy nuclei [25] and cluster radioactivity [44].

Without transfer channels, i.e., only low-energy excitations are included, our model is similar to the CCFUS model [32]. A difference arises from the treatment of the transmission coefficient below barrier. In our model we use the WKB approximation and calculate the transmission coefficient using the action integral, whereas in the CCFUS model the Hill-Wheeler approximation [39] is used. The difference related to the different parametrization of the nuclear part of the potential in both models can be evaluated, because this parametrization can be easily exchanged. Without transfer channels, our and the CCFUS model lead to similar results.

In our model, the capture process, the first step in the synthesis of SHEs by cold fusion, is enhanced by both the low-energy surface vibration in, and the neutron transfer between target and projectile. The energy, deformation length and multipolarity of the surface vibrations are determined by

nuclear structure effects. They also influence the separation energy of transferred neutrons and the reaction  $Q$  value. Therefore, in the survey of cross-section calculations as given later, it will be interesting to establish nuclear structure effects for the barrier transmission resulting from the capture step of the reaction.

The importance of subbarrier nucleon transfer channels for the synthesis of SHEs was already pointed out in [2,35].

### III. FORMATION OF THE NEAR SPHERICAL COMPOUND NUCLEUS

The shape of the fusing system after barrier penetration, i.e., at the inner turning point, is not much different from that of two spherical nuclei at the touching point. It is elongated, asymmetric and laced. From such a configuration the system develops further into the direction of a near spherical compound nucleus and later to the ground state, which can be deformed or spherical. This shape evolution is described by the equation

$$R(\vartheta) = R(\{\beta\}) \left[ 1 + \sum_{l=2}^N \beta_l Y_{l0}(\vartheta) \right]. \quad (20)$$

Near the inner turning point, the deformation parameters have rather big values,  $\beta_2 \approx 1.9$ ,  $\beta_3 \approx 0.25$ ,  $\beta_4 \approx -0.4$ , ... in the case of colliding spherical nuclei with atomic weights  $A_1 \approx 64$  and  $A_2 \approx 208$ . The values of the deformation parameters of SHEs in the ground state are  $\beta_2 \approx 0 - 0.3$  and  $\beta_{3,4,\dots} \approx 0$ ; see also Table I. The deformation parameters change significantly during the development to a spherical configuration. Note that the radial vector  $R(\{\beta\})$  in Eq. (20) depends on the deformation parameters  $\{\beta\} = \beta_2, \beta_3, \beta_4, \dots, \beta_N$  due to the volume conservation filled by the nuclear matter at variation of  $\{\beta\}$ .

The series (20) converges badly for asymmetric shapes. Nevertheless, we try to find a parameter set  $\beta_2, \beta_3, \beta_4, \dots, \beta_9$  describing two touching spherical nuclei with maximal accuracy, which is possible to reach by using the parametrization (20) and  $\beta_2, \beta_3, \beta_4, \dots, \beta_9$ . Then, the description by using Eq. (20) for two touching spheres is sufficient.

We assume that during the development to sphericity the even and odd deformation parameters change by the same factors  $p$  and  $q$ , respectively,  $p\beta_2, q\beta_3, p\beta_4, q\beta_5, \dots, q\beta_9$ . In the case of high asymmetry, the parameters are  $p, q \approx 1$  and near sphericity  $p, q \approx 0$ . The parameters  $p$  and  $q$  are connected to the elongation and asymmetry degrees of freedom of the nuclear shape during the formation of the spherical compound nucleus, respectively.

The potential energy surface for the nuclei  $^{258}\text{Rf}$ ,  $^{266}\text{Hs}$ ,  $^{272}\text{110}$ ,  $^{278}\text{112}$ ,  $^{286}\text{114}$  and  $^{290}\text{116}$  formed in reactions  $^{50}\text{Ti}$ ,  $^{58}\text{Fe}$ ,  $^{64}\text{Ni}$ ,  $^{70}\text{Zn}$ ,  $^{78}\text{Ge}$ ,  $^{82}\text{Se} + ^{208}\text{Pb}$ , respectively, is presented in Fig. 1. Although the shape parametrization (20) is too rough at large values of  $\beta_2$  and  $\beta_3$ , it is possible to study the inner barrier  $B_{\text{Sph}}$ , which has to be bypassed or crossed during the process of sphere formation. There, the  $\beta_2$  and  $\beta_3$  values are smaller,  $\beta_2 \approx 0.6 - 1.0$  and  $\beta_3 < 0.25$ , as shown in Fig. 1.

TABLE I. The parameters of ground-state and saddle-point properties of the compound nucleus (CN) and of evaporation residues (SHEs, after neutron emission). The fitting parameter  $c_v$  is also given (see text).

| Reaction                            | CN                 | $E_{nbe}^{CN}$<br>(MeV) | $\delta E_{shel}^{CN}$<br>(MeV) | $\beta_{2\text{ g.s.}}$ | $B_{CN}$<br>(MeV) | $\beta_{2\text{ sadl}}$ | $E_{n\text{ sep}}^{CN}$<br>(MeV) | $\log_{10} T_{sf}^a$ | SHEs               | $\delta E_{shel}^{SHE}$<br>(MeV) | $B_{SHE}$<br>(MeV) | $\gamma$<br>(MeV) <sup>-1</sup> | $c_v$ |
|-------------------------------------|--------------------|-------------------------|---------------------------------|-------------------------|-------------------|-------------------------|----------------------------------|----------------------|--------------------|----------------------------------|--------------------|---------------------------------|-------|
| <sup>58</sup> Fe+ <sup>207</sup> Pb | <sup>265</sup> 108 | -1931.90                | -5.21                           | 0.242                   | 5.60              | 0.475                   | 6.86                             | -0.73                | <sup>264</sup> 108 | -4.86                            | 5.5                | 0.09                            | 1.20  |
| <sup>64</sup> Ni+ <sup>207</sup> Pb | <sup>271</sup> 110 | -1964.76                | -6.34                           | 0.227                   | 5.25              | 0.468                   | 6.90                             | 1.24                 | <sup>270</sup> 110 | -5.85                            | 4.9                | 0.11                            | 1.10  |
| <sup>70</sup> Zn+ <sup>207</sup> Pb | <sup>277</sup> 112 | -1995.40                | -5.77                           | 0.204                   | 4.25              | 0.445                   | 6.16                             | -0.27                | <sup>276</sup> 112 | -5.92                            | 4.4                | 0.12                            | 0.98  |
| <sup>78</sup> Ge+ <sup>207</sup> Pb | <sup>285</sup> 114 | -2035.16                | -7.41                           | 0.132                   | 3.20              | 0.418                   | 6.41                             | -0.88                | <sup>284</sup> 114 | -7.00                            | 3.1                | 0.12                            | 0.98  |
| <sup>50</sup> Ti+ <sup>208</sup> Pb | <sup>258</sup> 104 | -1903.29                | -4.49                           | 0.248                   | 6.9               | 0.475                   | 7.72                             | -1.56                | <sup>258</sup> 104 | -4.68                            | 6.95               | 0.05                            | 1.35  |
| <sup>54</sup> Cr+ <sup>208</sup> Pb | <sup>262</sup> 106 | -1921.75                | -4.43                           | 0.244                   | 6.3               | 0.48                    | 7.74                             | -1.07                | <sup>265</sup> 108 | -4.93                            | 6.5                | 0.064                           | 1.20  |
| <sup>58</sup> Fe+ <sup>208</sup> Pb | <sup>266</sup> 108 | -1940.13                | -5.27                           | 0.241                   | 5.7               | 0.48                    | 8.23                             | 0.21                 | <sup>265</sup> 108 | -5.21                            | 5.6                | 0.09                            | 1.20  |
| <sup>59</sup> Co+ <sup>208</sup> Pb | <sup>267</sup> 109 | -1940.57                | -5.41                           | 0.235                   | 5.0               | 0.47                    | 8.22                             | -1.47                | <sup>266</sup> 109 | -5.39                            | 4.85               | 0.09                            | 1.20  |
| <sup>62</sup> Ni+ <sup>208</sup> Pb | <sup>270</sup> 110 | -1957.86                | -5.85                           | 0.227                   | 4.9               | 0.465                   | 8.54                             | -0.27                | <sup>269</sup> 110 | -5.60                            | 4.6                | 0.11                            | 1.10  |
| <sup>64</sup> Ni+ <sup>208</sup> Pb | <sup>272</sup> 110 | -1973.03                | -6.55                           | 0.226                   | 5.6               | 0.47                    | 8.27                             | 2.75                 | <sup>271</sup> 110 | -6.34                            | 5.25               | 0.11                            | 1.10  |
| <sup>65</sup> Cu+ <sup>208</sup> Pb | <sup>273</sup> 111 | -1973.14                | -6.41                           | 0.224                   | 5.05              | 0.465                   | 8.29                             | 1.78                 | <sup>272</sup> 111 | -6.20                            | 4.68               | 0.11                            | 1.10  |
| <sup>66</sup> Zn+ <sup>208</sup> Pb | <sup>274</sup> 112 | -1974.51                | -5.91                           | 0.221                   | 4.5               | 0.46                    | 8.66                             | -0.20                | <sup>273</sup> 112 | -5.67                            | 4.1                | 0.12                            | 0.98  |
| <sup>68</sup> Zn+ <sup>208</sup> Pb | <sup>276</sup> 112 | -1989.24                | -5.92                           | 0.206                   | 4.4               | 0.45                    | 7.93                             | 0.13                 | <sup>275</sup> 112 | -6.17                            | 4.45               | 0.12                            | 0.98  |
| <sup>70</sup> Zn+ <sup>208</sup> Pb | <sup>278</sup> 112 | -2002.64                | -5.06                           | 0.202                   | 4.1               | 0.44                    | 7.24                             | -0.67                | <sup>277</sup> 112 | -5.77                            | 4.25               | 0.12                            | 0.98  |
| <sup>71</sup> Ga+ <sup>208</sup> Pb | <sup>279</sup> 113 | -2002.89                | -5.11                           | 0.196                   | 3.8               | 0.44                    | 7.46                             | -1.92                | <sup>278</sup> 113 | -5.62                            | 3.9                | 0.12                            | 0.98  |
| <sup>74</sup> Ge+ <sup>208</sup> Pb | <sup>282</sup> 114 | -2020.67                | -6.57                           | 0.182                   | 3.2               | 0.425                   | 8.17                             | -2.33                | <sup>281</sup> 114 | -6.47                            | 3.35               | 0.12                            | 0.98  |
| <sup>76</sup> Ge+ <sup>208</sup> Pb | <sup>284</sup> 114 | -2035.16                | -7.00                           | 0.143                   | 3.1               | 0.415                   | 7.89                             | -1.93                | <sup>283</sup> 114 | -6.95                            | 3.15               | 0.12                            | 0.98  |
| <sup>78</sup> Ge+ <sup>208</sup> Pb | <sup>286</sup> 114 | -2049.15                | -7.36                           | 0.121                   | 3.3               | 0.41                    | 7.58                             | 0.17                 | <sup>285</sup> 114 | -7.41                            | 3.2                | 0.12                            | 0.98  |
| <sup>75</sup> As+ <sup>208</sup> Pb | <sup>283</sup> 115 | -2020.85                | -6.95                           | 0.179                   | 3.15 <sup>b</sup> | 0.42                    | 8.18                             | -3.52                | <sup>282</sup> 115 | -6.86                            | 3.1 <sup>b</sup>   | 0.12                            | 0.98  |
| <sup>80</sup> Se+ <sup>208</sup> Pb | <sup>288</sup> 116 | -2051.87                | -7.50                           | 0.077                   | 4.3 <sup>b</sup>  | 0.40                    | 7.87                             | -3.48                | <sup>287</sup> 116 | -7.60                            | 3.9 <sup>b</sup>   | 0.12                            | 0.98  |
| <sup>82</sup> Se+ <sup>208</sup> Pb | <sup>290</sup> 116 | -2066.05                | -7.81                           | 0.075                   | 5.1 <sup>b</sup>  | 0.39                    | 7.72                             | 2.87                 | <sup>289</sup> 116 | -7.83                            | 4.7 <sup>b</sup>   | 0.12                            | 0.98  |
| <sup>58</sup> Fe+ <sup>210</sup> Pb | <sup>268</sup> 108 | -1955.01                | -5.95                           | 0.237                   | 6.1               | 0.47                    | 8.13                             | 1.98                 | <sup>267</sup> 108 | -5.75                            | 5.90               | 0.09                            | 1.20  |
| <sup>64</sup> Ni+ <sup>210</sup> Pb | <sup>274</sup> 110 | -1986.88                | -6.40                           | 0.217                   | 5.2               | 0.46                    | 7.43                             | 1.68                 | <sup>273</sup> 108 | -6.79                            | 5.40               | 0.11                            | 1.10  |
| <sup>70</sup> Zn+ <sup>210</sup> Pb | <sup>280</sup> 112 | -2016.55                | -5.17                           | 0.191                   | 3.6               | 0.43                    | 7.75                             | -1.07                | <sup>279</sup> 112 | -5.14                            | 3.85               | 0.12                            | 0.98  |
| <sup>78</sup> Ge+ <sup>210</sup> Pb | <sup>288</sup> 114 | -2062.78                | -7.80                           | 0.086                   | 4.1               | 0.40                    | 7.46                             | 3.32                 | <sup>287</sup> 114 | -7.74                            | 3.7                | 0.12                            | 0.98  |
| <sup>50</sup> Ti+ <sup>209</sup> Bi | <sup>259</sup> 105 | -1904.85                | -4.91                           | 0.248                   | 6.65              | 0.475                   | 7.78                             | -1.68                | <sup>258</sup> 105 | -5.07                            | 6.68               | 0.05                            | 1.35  |
| <sup>54</sup> Cr+ <sup>209</sup> Bi | <sup>263</sup> 107 | -1923.01                | -5.17                           | 0.243                   | 5.9               | 0.475                   | 7.93                             | -1.37                | <sup>262</sup> 107 | -5.31                            | 5.9                | 0.064                           | 1.20  |
| <sup>58</sup> Fe+ <sup>209</sup> Bi | <sup>267</sup> 109 | -1940.57                | -5.41                           | 0.235                   | 5.0               | 0.471                   | 8.22                             | -1.47                | <sup>266</sup> 109 | -5.39                            | 4.8                | 0.09                            | 1.20  |
| <sup>59</sup> Co+ <sup>209</sup> Bi | <sup>268</sup> 110 | -1942.15                | -5.07                           | 0.229                   | 4.3               | 0.46                    | 8.68                             | -3.14                | <sup>262</sup> 107 | -4.93                            | 4.1                | 0.09                            | 1.20  |
| <sup>64</sup> Ni+ <sup>209</sup> Bi | <sup>273</sup> 111 | -1973.14                | -6.41                           | 0.224                   | 5.05              | 0.465                   | 8.29                             | 1.28                 | <sup>272</sup> 111 | -6.20                            | 4.68               | 0.11                            | 1.10  |
| <sup>70</sup> Zn+ <sup>209</sup> Bi | <sup>279</sup> 113 | -2002.89                | -5.11                           | 0.196                   | 3.8               | 0.44                    | 7.46                             | -1.92                | <sup>278</sup> 113 | -5.62                            | 3.9                | 0.12                            | 0.98  |
| <sup>78</sup> Ge+ <sup>209</sup> Bi | <sup>287</sup> 115 | -2050.04                | -7.76                           | 0.099                   | 3.8 <sup>b</sup>  | 0.405                   | 7.56                             | 0.28                 | <sup>286</sup> 115 | -7.84                            | 3.55               | 0.12                            | 0.98  |

<sup>a</sup>The  $T_{sf}$  is in sec.<sup>b</sup>The dynamic fission barrier(s) [17,18] is (are) used in the estimation of the static fission barrier.

The macroscopic energies and shell correction energies as function of the parameters  $p$  and  $q$  in the deformation space  $p\beta_2, q\beta_3, p\beta_4, q\beta_5, \dots, q\beta_9$  were calculated by using the computer code WSBETA [45]. The code uses a Woods-Saxon potential with a ‘‘universal’’ parameter set [45], and 19 harmonic oscillator shells are taken into account for the calculation of the eigenvalues. The residual pairing interaction is calculated by means of the Lipkin-Nogami method [46]. The macroscopic part of the deformation energy is evaluated using the Yukawa-plus-exponential potential [47].

Especially important in the calculations of the fusion and fission barriers is the dependence of the shell-correction energy from the nuclear temperature. In the first step of the reaction, the crossing of the fusion barrier, the system is not strongly heated. The reason is that the collective velocities are rather small for cold fusion at subbarrier energies. This is different after crossing the inner barrier  $B_{Sph}$ . Then, the

nuclear temperature is high, and the shell-correction energy is severely washed out. As a consequence, the fission barrier decreases and the ratio between fission and neutron evaporation increases. More details are given in the next section.

For all cases shown in Fig. 1, there exists a barrier  $B_{Sph}$  between the configuration of two touching spheres and the spherical or near spherical compound nucleus. The height of the barrier is increasing with the atomic number. A similar result was obtained by another investigation, however, with a different parametrization for both the mean field potential and the shape evolution [22,23].

Note that due to bad convergency of the series (20) and relative restriction between even and odd deformations in Eq. (20) during shape evolution our estimation of the inner barrier has of qualitative character. Exact calculation of this inner barrier is very difficult. Our calculation has qualitative sense and gives the upper limit of this barrier.

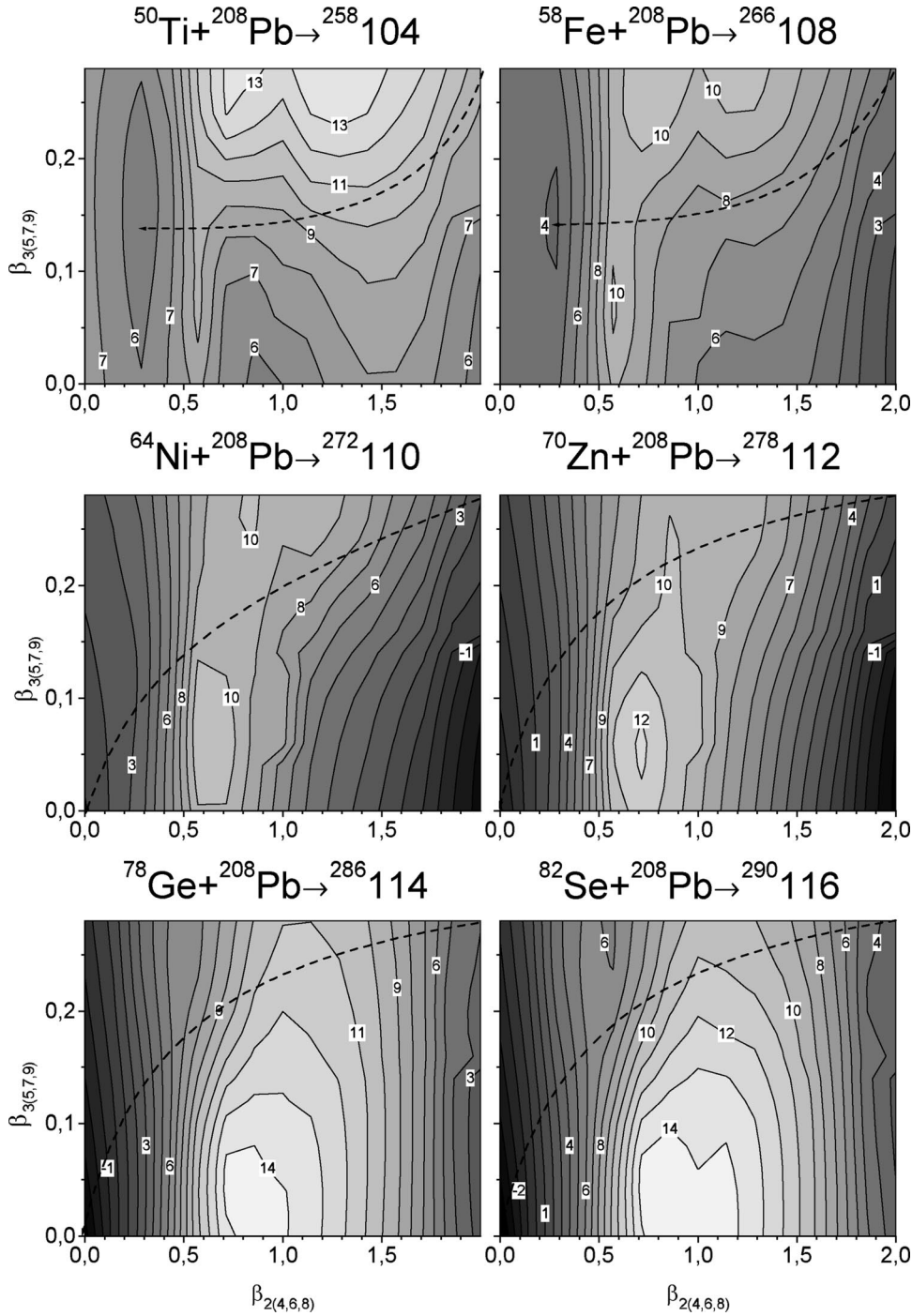


FIG. 1. Potential energy surfaces as function of the deformation parameters  $\beta$  for cold fusion reactions from  $^{50}\text{Ti} + ^{208}\text{Pb} \rightarrow ^{258}104$  to  $^{82}\text{Se} + ^{208}\text{Pb} \rightarrow ^{290}116$ . In each graph is the touching configuration of the spherical projectile and target nucleus close to the upper right corner and that of the ground state close to bottom left. The dashed line is the tunneling trajectory which is drawn by eye and by using the proposal that all deformations are monotonously changed during motion to equilibrium compound nucleus shape. The ratio between even and odd deformation parameters is fixed; see text for details. The contour lines are drawn in steps of 1 MeV; the maximum values and several others are given in MeV on each graph.

The barrier height for the reaction  $^{70}\text{Zn} + ^{208}\text{Pb} \rightarrow ^{278}112$  is  $B_{\text{Sph}} \approx 13.5$  MeV in our calculation. This value is close to that one obtained in [22,23]. The potential energy surface for the reaction  $^{50}\text{Ti} + ^{208}\text{Pb} \rightarrow ^{258}\text{Rf}$  does not show a pronounced barrier between the two touching sphere configuration and the spherical compound nucleus, however, in this system we find a pronounced minimum for the deformed ground state at  $\beta_2 \approx 0.2 - 0.3$ . A similar structure of the potential energy surface for the reaction  $^{50}\text{Ti} + ^{208}\text{Pb} \rightarrow ^{258}\text{Rf}$  was also observed in [22].

The transmission coefficient  $T_S(E, B_{\text{Sph}})$  for the barrier penetration during the shape evolution from the touching

projectile and target nuclei to the near spherical shape of the compound nucleus were estimated in the Hill-Wheeler approximation [39] for various collision energies  $E$ . The value of the barrier height  $B_{\text{Sph}}$  was extracted from Fig. 1. For the curvature of the barrier we used 1 MeV in the case of the deformed SHEs and increased this value up to 3 MeV for the spherical SHEs.

As will be shown later, the inner barrier  $B_{\text{Sph}}$  is less important in cold fusion leading to SHEs with  $Z \leq 110$ , because the lowest collision energies used experimentally [2] were above the height of the barrier and already on the decreasing slope of the excitation function. However, the inner barrier

becomes significant for the formation of SHEs with  $Z \geq 112$  at low collision energies.

#### IV. COMPETITION BETWEEN NEUTRON EVAPORATION AND FISSION

After the first two steps of the reaction, the transmission through the fusion and the inner barrier, a compound nucleus of atomic weight  $A$  is formed with equilibrium deformation

near sphericity and excitation energy  $E^*$ . The dominant decay modes of a heavy compound nucleus at low excitation energy, as it is the case in cold fusion, are the evaporation of neutrons and the fission. The residue of mass  $A-1$  after neutron emission may still be excited. Again, it may fission or cool down by emission of  $\gamma$ 's. Therefore, the survival probability in the formation process from a compound nucleus to a residue with charge  $Z$ , atomic mass  $A-1$  and angular momentum  $l$  is equal to

$$\mathcal{W}(E, l) = \frac{\Gamma_{\text{SHE}}(E + Q_{\text{fus}}, l, A, Z)}{\Gamma_{\text{n}}(E + Q_{\text{fus}}, l, A, Z) + \Gamma_{\text{fis}}(E + Q_{\text{fus}}, l, A, Z)}, \quad (21)$$

where

$$\Gamma_{\text{n}}(E + Q_{\text{fus}}, l, A, Z) = \frac{1}{2\pi\rho(E + Q_{\text{fus}}, l, A, Z, \beta_{\text{g.s.}})} \int_0^{E + Q_{\text{fus}} + E_{\text{sep}}} d\varepsilon \sum_{j_n} \rho(E + Q_{\text{fus}} + E_{\text{sep}} - \varepsilon, |\mathbf{l} - \mathbf{j}_n|, A - 1, Z, \beta_{\text{g.s.}}) T_{\text{n}} \times (E + Q_{\text{fus}}, \varepsilon, l_n, j_n, A, Z) \quad (22)$$

is the width of neutron emission [10],

$$\Gamma_{\text{fis}}(E + Q_{\text{fus}}, l, A, Z) = \frac{1}{2\pi\rho(E + Q_{\text{fus}}, l, A, Z, \beta_{\text{g.s.}})} \int_0^{E + Q_{\text{fus}}} d\varepsilon \rho(\varepsilon, l, A - 1, Z, \beta_{\text{sadl}}) T_{\text{fis}}(E + Q_{\text{fus}}, \varepsilon, B_{\text{CN}}^*, l, A, Z) \quad (23)$$

is the fission width [10], and

$$\Gamma_{\text{SHE}}(E + Q_{\text{fus}}, l, A, Z) = \frac{1}{2\pi\rho(E + Q_{\text{fus}}, l, A, Z, \beta_{\text{g.s.}})} \int_0^{E + Q_{\text{fus}} - E_{\text{sep}}} d\varepsilon \sum_{j_n} \rho(E + Q_{\text{fus}} - E_{\text{sep}} - \varepsilon, |\mathbf{l} - \mathbf{j}_n|, A - 1, Z, \beta_{\text{g.s.}}) T_{\text{n}}(E + Q_{\text{fus}}, \varepsilon, l_n, j_n, A, Z) \frac{\Gamma_{\gamma}(E + Q_{\text{fus}} - E_{\text{sep}} - \varepsilon, |\mathbf{l} - \mathbf{j}_n|, A - 1, Z)}{\Gamma_{\gamma}(E + Q_{\text{fus}} - E_{\text{sep}} - \varepsilon, |\mathbf{l} - \mathbf{j}_n|, A - 1, Z) + \Gamma_{\text{fis}}(E + Q_{\text{fus}} - E_{\text{sep}} - \varepsilon, |\mathbf{l} - \mathbf{j}_n|, A - 1, Z)} \quad (24)$$

is the width of formation of SHE in the ground state.  $E$  is the collision energy in the center of mass system and  $Q_{\text{fus}}$  is the fusion-reaction  $Q$  value [see also Eq. (18)].  $E_{\text{sep}}$  is the neutron separation energy,  $B_{\text{CN}}^*$  and  $B_{\text{SHE}}^*$  are the saddle point energy of the compound nucleus and of the residue after neutron emission used for evaluation of  $\Gamma_{\text{fis}}$  in Eqs. (21) and (24), respectively,

$$\Gamma_{\gamma}(E^*, j_i, A, Z) = \int d\varepsilon \sum_{j_f=|j_i-1|}^{j_f=|j_i+1|} \frac{\rho(E^* - \varepsilon, j_f, A, Z, \beta_{\text{g.s.}})}{\rho(E^*, j_i, A, Z, \beta_{\text{g.s.}})} \frac{3.31 \times 10^{-6} \text{ MeV}(A - Z)Z\varepsilon^4 \Gamma}{A[(E_0^2 - \varepsilon^2)^2 - (\varepsilon\Gamma)^2]} \quad (25)$$

is the width of  $\gamma$  emission [27,48].  $E_0 \approx 80A^{1/3}$  MeV and  $\Gamma \approx 5$  MeV are the energy and the width of the giant dipole resonance, respectively.

The transmission coefficient of the neutron emission  $T_{\text{n}}(\varepsilon, l_n, j_n, A, Z)$  used in Eqs. (22) and (24) is calculated in the WKB approximation [38] using the Becchetti-Greenlees neutron-nucleus potential [49].

The fission transmission coefficient  $T_{\text{fis}}(E^*, \varepsilon, B^*, A, Z)$  in Eq. (23) of a nucleus at excitation energy  $E^*$  is calculated by using the Hill-Wheeler approximation [39],

$$T_{\text{fis}}(E + Q_{\text{fus}}, \varepsilon, B^*, l, A, Z) = 1/[1 + \exp(2\pi(\varepsilon - B^*)/(\hbar\omega))]. \quad (26)$$

The curvature  $\hbar\omega$  of the fission barrier depends from the spontaneous-fission lifetime  $T_{\text{sf}}$  of the ground state

$$\hbar\omega = 2\pi B/\ln(T_{\text{sf}}/T_0 - 1)$$

and from  $T_0 = 2\pi(\ln 2)\hbar/E_{\text{zp}}$ . Here, we take the same value of the zero point energy  $E_{\text{zp}} = 0.7$  MeV as in [17,18].

The fission of an excited nucleus is an isoentropic process [24,26]. According to Strutinsky's shell-correction method [8], the fission barrier  $B^*$  of an excited nucleus at  $l=0$  is given by

$$B^* = [\mathcal{E}_{\text{sadl}}^{\text{macro}} + \delta\mathcal{E}_{\text{sadl}}^{\text{shell}}(E^*)] - [\mathcal{E}_{\text{g.s.}}^{\text{macro}} + \delta\mathcal{E}_{\text{g.s.}}^{\text{shell}}(E^*)], \quad (27)$$

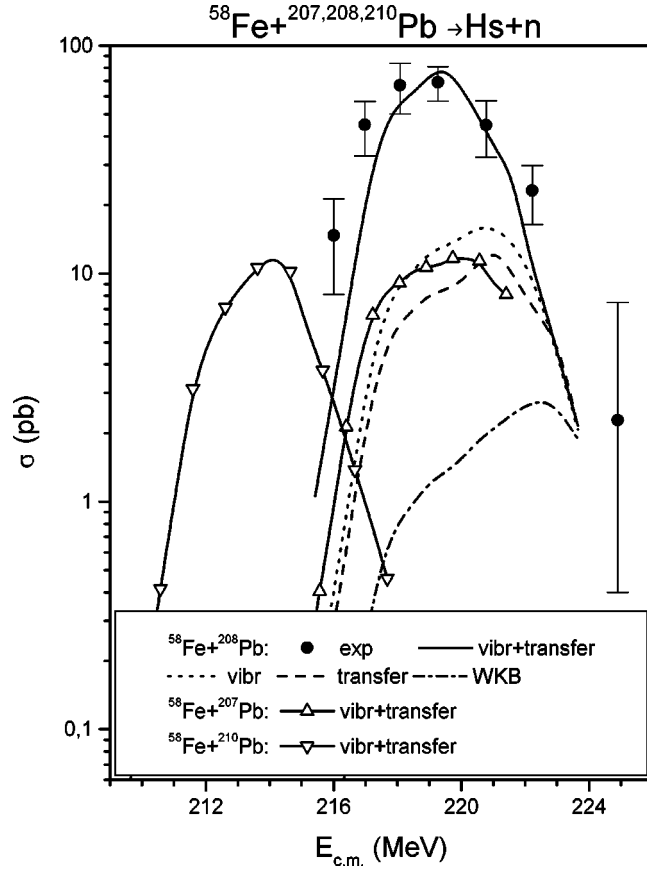


FIG. 2. Calculated excitation functions for the reactions  $^{58}\text{Fe} + {}^{207,208,210}\text{Pb} \rightarrow {}^{264,265,267}\text{Hs} + n$ . The continuous curve shows the results for the reaction  $^{58}\text{Fe} + {}^{208}\text{Pb} \rightarrow {}^{265}\text{Hs} + n$  taking into account both the low-energy  $2^+$  and  $3^-$  vibrations and the neutron transfer channels. The dotted and the dashed curves show the results for considering solely the  $2^+$  and  $3^-$  vibrations and the neutron transfer channels, respectively. The result of the one-dimensional WKB approach is shown by the dash-dotted curve. The data obtained for the reaction  $^{58}\text{Fe} + {}^{207}\text{Pb} \rightarrow {}^{264}\text{Hs} + n$  are represented by ( $\Delta$ ) and those for  $^{58}\text{Fe} + {}^{210}\text{Pb} \rightarrow {}^{267}\text{Hs} + n$  by ( $\nabla$ ). In both cases only the results including vibrations and transfer are shown. The relations taking into account the channels separately are similar as in the case of  $^{58}\text{Fe} + {}^{208}\text{Pb}$ . The experimental data shown here and in Figs. 3 – 6 and 9 – 12 are from [2].

where  $\mathcal{E}_{\text{sadl}}^{\text{macro}}$  and  $\mathcal{E}_{\text{g.s.}}^{\text{macro}}$  are the macroscopic energies calculated for the nucleus at deformation of the saddle point and the ground state, respectively. We rewrite Eq. (27) in the form

$$B^* \approx [\mathcal{E}_{\text{sadl}}^{\text{macro}} - \mathcal{E}_{\text{g.s.}}^{\text{macro}}] - \delta\mathcal{E}_{\text{g.s.}}^{\text{shell}}(E^*), \quad (28)$$

because the shell-correction energy at the saddle point is close to zero [53].

The shell-correction energy of excited nuclei is smaller as in the ground state, it decreases with increasing excitation energy  $E^*$  [24,26,27,50,51,54–56]. The following ansatz is used [27,54,55]:

$$\delta\mathcal{E}^{\text{shell}}(E^*) = \delta\mathcal{E}^{\text{shell}}(0)f(E^*), \quad (29)$$

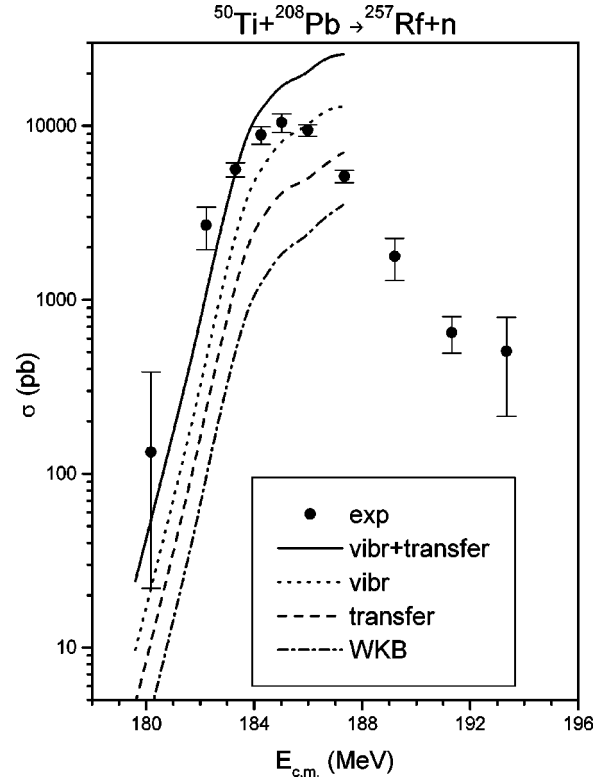


FIG. 3. Calculated excitation functions for the reaction  $^{50}\text{Ti} + {}^{208}\text{Pb} \rightarrow {}^{257}\text{Rf} + n$ . For the calculations the assignment of the curves is the same as in Fig. 2.

where [27,55]

$$f(E^*) = \exp(-\gamma E^*). \quad (30)$$

The value of the shell-correction damping parameter  $\gamma$  in Eq. (30) is not well known. For example, the two different values  $\gamma = 0.064$  MeV [54] and  $\gamma = 0.05$  MeV [55] were adjusted for shell correction washing out effect in energy level density for nuclei in the lead region. The damping parameter  $\gamma$  depends also on the proton and neutron number; see [24,56] for details.

The macroscopic contribution  $\mathcal{E}_{\text{sadl}}^{\text{macro}} - \mathcal{E}_{\text{g.s.}}^{\text{macro}}$  to the fission barrier is close to zero or even negative. The fission barrier is determined by the (negative) shell-correction energy at ground-state deformation, which disappears with increasing excitation energy. Therefore, fission is the main decay mode of excited heavy nuclei.

Rotation of the compound nucleus leads to a reduction of the fission barrier, because the moment inertia is smaller for the ground state than for the strongly deformed nucleus at the saddle point. The fission barrier of the excited rotating nucleus is equal to

$$B^* \approx [\mathcal{E}_{\text{sadl}}^{\text{macro}} - \mathcal{E}_{\text{g.s.}}^{\text{macro}}] - \delta\mathcal{E}_{\text{g.s.}}^{\text{shell}}f(E^*) - \frac{\hbar^2 l(l+1)}{2[\kappa(^2/5mr_0^2A^{5/2})]} \left( \frac{1}{1+\beta_{2,\text{g.s.}}} - \frac{1}{1+\beta_{2,\text{sadl}}} \right). \quad (31)$$

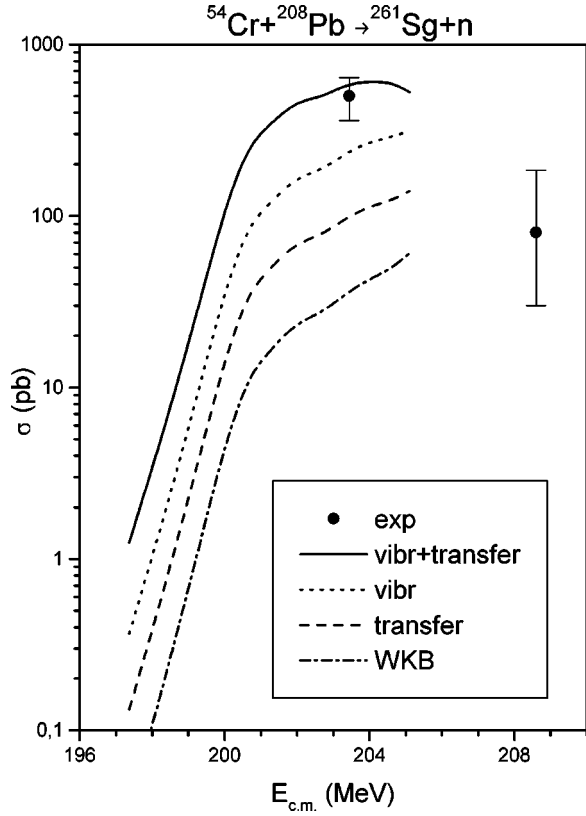


FIG. 4. Calculated excitation functions for the reaction  $^{54}\text{Cr} + ^{208}\text{Pb} \rightarrow ^{261}\text{Sg} + n$ . For the calculations the assignment of the curves is the same as in Fig. 2.

We chose  $\kappa=0.3$  in Eq. (31) for adjusting the rigid-body moment of inertia  $^{2/5}mr_0^2A^{5/2}(1+\beta_2)$  to the realistic value.

We rewrite the last equation into the form

$$B^* \approx B + \delta\mathcal{E}_{\text{g.s.}}^{\text{shell}}(1-f(E^*)) - \frac{\hbar^2 l(l+1)}{2[\kappa(^{2/5}mr_0^2A^{5/2})]} \times \left( \frac{1}{1+\beta_{2,\text{g.s.}}} - \frac{1}{1+\beta_{2,\text{sadl}}} \right), \quad (32)$$

in order to make use of literature values [8,9,16–27] for the fission barrier  $B$  of the nucleus in the ground state and of the shell correction energy  $\delta\mathcal{E}_{\text{g.s.}}^{\text{shell}}$ . The used values are given in Table I.

The energy level density  $\rho(E^*, j_f, A, Z, \beta_2)$  introduced in Eqs. (21)–(24) is calculated according to Ignatyuk *et al.* [52]

$$\rho(E^*, l, A, Z, \beta_2) = \rho_{\text{BCS}}(E^*, l, A, Z) K_{\text{coll}}(E^*, A) K_{\text{rot}}(E^*, A, \beta_2), \quad (33)$$

where  $\rho_{\text{BCS}}$  is the density of noncollective nuclear excitations,  $K_{\text{coll}}(E^*, A)$  and  $K_{\text{rot}}(E^*, A)$  are the coefficients of the level density enhancement due to the vibrational and rotational collective motion, respectively. We use the parameters of the energy level density (33) as recommended in [52].

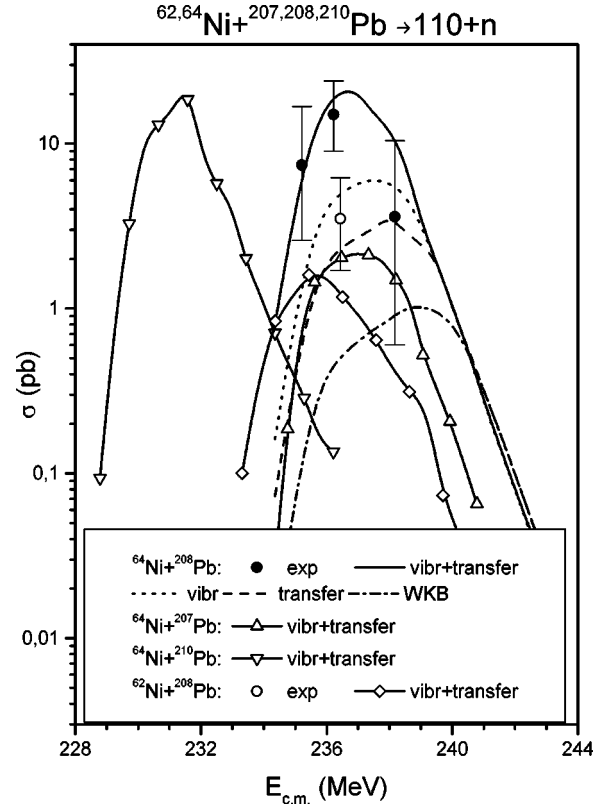


FIG. 5. Calculated excitation functions for the reactions  $^{62,64}\text{Ni} + ^{207,208,210}\text{Pb} \rightarrow 110 + n$ . The notation for the reactions  $^{64}\text{Ni} + ^{207,208,210}\text{Pb}$  corresponds to  $^{58}\text{Fe} + ^{207,208,210}\text{Pb}$  in Fig. 2. The inset explains the assignment of the reactions to the symbols.

Note that the energy level density depends on the quadrupole deformation  $\beta_2$  and is therefore different for the ground-state and the saddle point.

Considering all effects discussed in Secs. II–IV, we write the cross section for the formation of SHEs in cold fusion at a kinetic energy  $E$  in the form

$$\sigma_{\text{SHE}}(E) = \frac{\pi\hbar^2}{2\mu E} \sum_l (2l+1) \sum_k |U_{k0}|^2 \left[ T(E, \mathcal{V}_{lk}^i) + \sum_f T(E, \mathcal{V}_{lk}^i, \mathcal{V}_{lk}^f) \right] T_{\text{S}}(E, B_{\text{Sph}}) \mathcal{W}(E, l). \quad (34)$$

## V. RESULTS AND DISCUSSION

The experimental investigation of excitation functions for the production of SHEs becomes increasingly difficult with increasing element number due to the decreasing cross sections. One of the heaviest systems studied experimentally over a wider range of excitation energy is  $^{58}\text{Fe} + ^{208}\text{Pb} \rightarrow ^{265}\text{Hs}^*$  [6], the data are shown in Fig. 2. The maximum of the excitation function is located at a collision energy  $E_{\text{cm}} \approx 218$  MeV and was assigned to the  $1n$ -evaporation channel. Only one data point was observed for the  $2n$  channel, which overlaps with the value at 225 MeV of the  $1n$  channel.

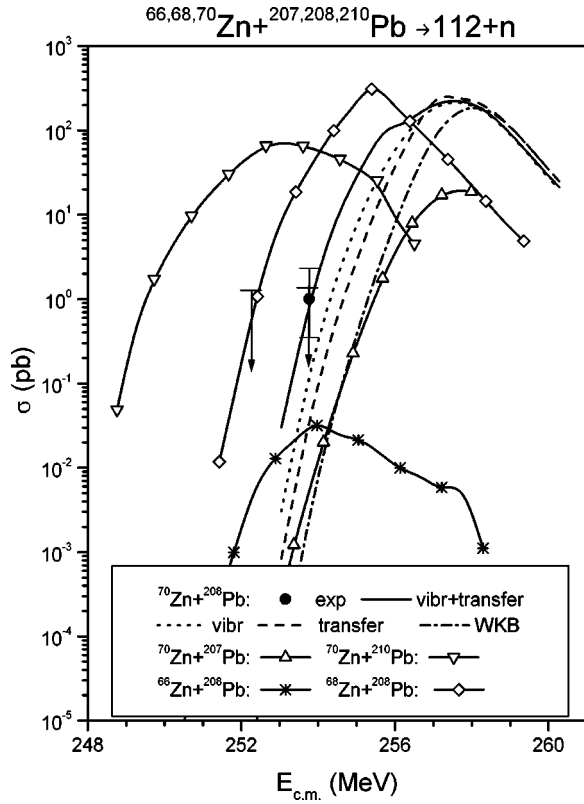


FIG. 6. Calculated excitation functions for the reactions  ${}^{66,68,70}\text{Zn} + {}^{207,208,210}\text{Pb} \rightarrow 112 + n$ . The notation for the reactions  ${}^{70}\text{Zn} + {}^{207,208,210}\text{Pb}$  corresponds to  ${}^{58}\text{Fe} + {}^{207,208,210}\text{Pb}$  in Fig. 2. The inset explains the assignment of the reactions to the symbols. The vertical arrows show the upper experimental limit of the cross section for the reaction  ${}^{68}\text{Zn} + {}^{208}\text{Pb} \rightarrow {}^{275}112 + n$ .

The full width at half maximum of the excitation function is approximately 4 MeV.

The experimental data are compared in Fig. 2 with several modifications of our model. In the simplest case, using tunneling through a one-dimensional barrier and the WKB method, the results strongly underestimate the experimental fusion cross sections. The position of the maximum of the excitation function is shifted into the direction of higher energy by about 3.5 MeV compared with the experimental value. Better agreement is obtained when the neutron transfer channels from lead to iron are taken into account. They occur with  $Q$  values of 1.3 MeV and 0.1 MeV for the  $2n$  and  $4n$  channels, respectively. We found, however, that the  $4n$  channel is negligible due to its low  $Q$  value. Similarly, the cross sections increase by including in the calculations the low-energy  $2^+$  and  $3^-$  surface vibrational excitations of both projectile and target. The best results are obtained by considering transfer and vibrations simultaneously.

The Krappe-Nix-Sierk potential [40] with the parameter set used in [43] was also used in our calculations of the nuclear part of the interaction. However, the strength constant was multiplied by a factor  $c_V$ , and also the radius parameter  $r_0$  was modified. The reason was that the barriers in the case of cold fusion are lower as in those cases, where the literature values were fitted. Using the original values of the parameters, the capture cross sections are too small and the

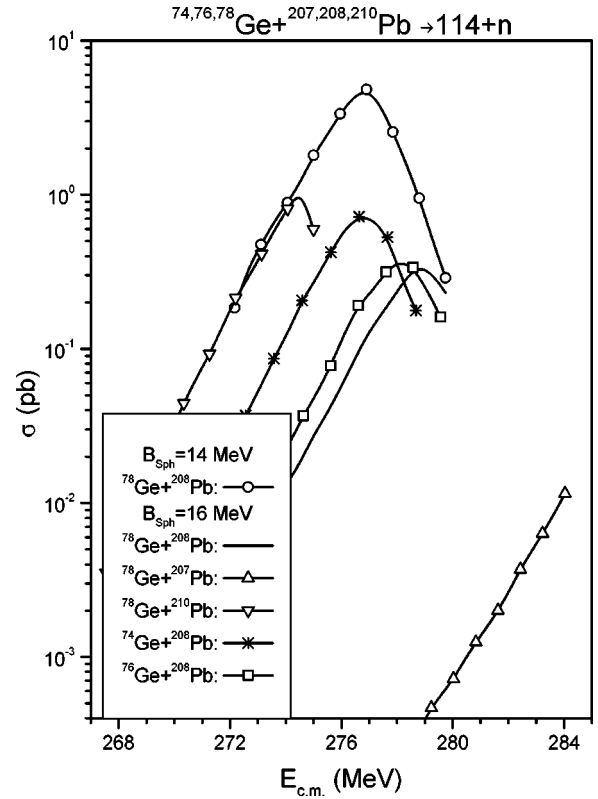


FIG. 7. Calculated excitation functions for the reactions  ${}^{74,76,78}\text{Ge} + {}^{207,208,210}\text{Pb} \rightarrow 114 + n$ . The inset explains the assignment of the reactions to the symbols. All curves on the plot include both vibrations and transfer. For these reactions the subbarrier enhancement is small and, therefore, the values taking into account the individual contributions are only slightly lower. A reduction of the barrier  $B_{\text{Sph}}$  by 2 MeV (see text) increases the cross section considerably, as shown by the two curves for the reaction  ${}^{78}\text{Ge} + {}^{208}\text{Pb} \rightarrow {}^{285}114 + n$ .

resulting fusion-evaporation cross sections do strongly underestimate the experimental data. This is the case also, when transfer and vibrations are included. With the original parameter set, the barrier seems to be overestimated by several MeV in the case of the synthesis of SHEs, a result, which was also taken into account in the calculations in [12]. For the radius parameter we used  $r_0 = 1.20$  fm for all nuclei considered here. This value is a slightly bigger than  $r_0 = 1.16$  as used in [43]. The value of the factors  $c_V$  used here are listed in Table I.

For the energies and the deformation parameters of the  $2^+$  and  $3^-$  vibrational states of the nuclei studied here, we took experimental data published in the literature [57–65]. In the case that no experimental values are known, we took the same values of energies and the deformation parameters of the  $2^+$  and  $3^-$  vibrational states as for neighboring isotopes.

The intrinsic barrier  $B_{\text{Sph}}$  on the way from the touching configuration to the near spherical compound nucleus is close to 6 MeV for the reaction  ${}^{58}\text{Fe} + {}^{208}\text{Pb} \rightarrow {}^{265}\text{Hs} + n$ ; see Fig. 1. This value is very close to the one obtained recently in [22,23]. The height of intrinsic barrier is equal to  $B_{\text{Sph}} - Q_{\text{fus}} \approx 6 \text{ MeV} + 206 \text{ MeV} = 212 \text{ MeV}$ . This value is smaller than the energy of 218 MeV measured for the maxi-

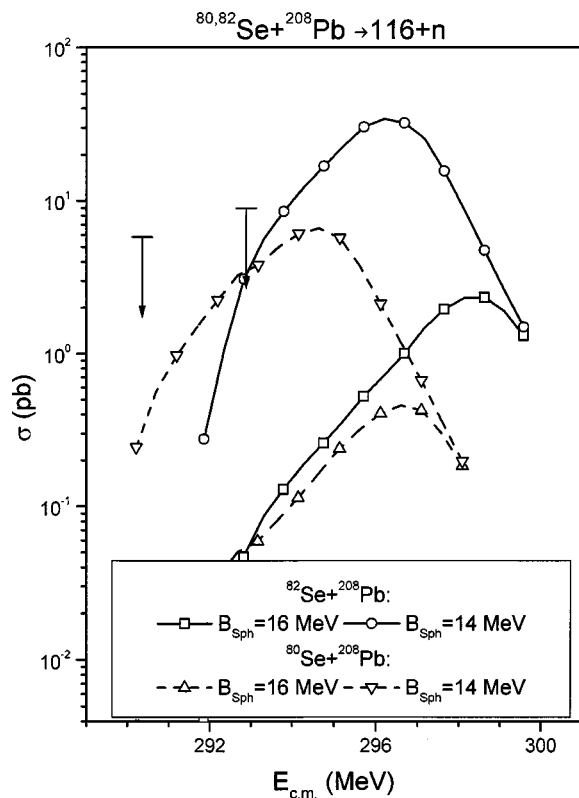


FIG. 8. Calculated excitation functions for the reactions  $^{80,82}\text{Se} + ^{208}\text{Pb} \rightarrow ^{287,289}\text{116} + n$ . The inset explains the assignment of the reactions to the symbols. All curves on the plot include both vibrations and transfer for the same reason as explained in Fig. 7. Also here, a reduction of the barrier  $B_{\text{Sph}}$  by 2 MeV (see text) increases the cross section considerably. The vertical arrows show the upper experimental limit of the cross section for the reaction  $^{82}\text{Se} + ^{208}\text{Pb} \rightarrow ^{289}\text{116} + n$ .

imum of the excitation function. Therefore, the intrinsic barrier is of minor importance for the reaction  $^{58}\text{Fe} + ^{208}\text{Pb}$ .

The important parameters, which determine the decay of the compound nucleus formed by cold fusion, are the quadrupole deformations in the ground state and in the saddle point, the fission barrier at zero excitation energy, the fission lifetime and the ground-state shell correction energy for the nuclei before and after neutron emission. The values for these parameters were taken from literature [16–20] and are listed in Table I. In the case of unavailable fission barriers (odd nuclei) and saddle-point deformations, we made an estimate by interpolation and with the help of the data shown in the graphs in [18–20].

The reduction of the cross section at low collision energy (Fig. 2) is related to the attenuation of the fusion barrier transmission. At high energy the cross sections decrease due to the decreasing survival probability of the compound nucleus. Because of the strong reduction of the fission barrier at increasing excitation energy, Eqs. (28)–(32), the fission width of the heated compound nucleus becomes much larger than the width for neutron evaporation. Therefore, the maximum of the excitation function shown in Fig. 2 originates from a balance between the fusion barrier transmission and the survival probability of the compound nucleus.

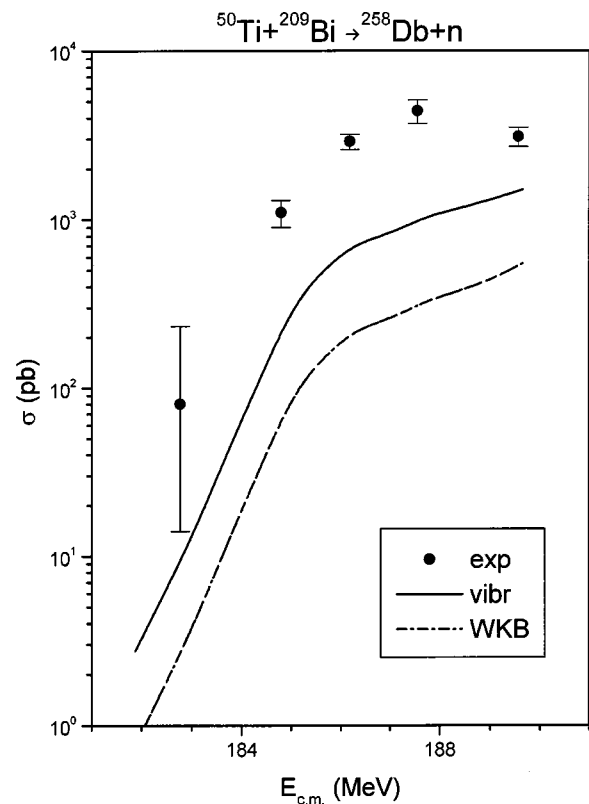


FIG. 9. Calculated excitation functions for the reaction  $^{50}\text{Ti} + ^{209}\text{Bi} \rightarrow ^{258}\text{Db} + n$ . The inset explains the assignment of the calculations to the curves. For this reaction, the subbarrier contribution due to transfer is negligibly small.

The results of the calculations for reactions between the projectiles  $^{50}\text{Ti}$ ,  $^{54}\text{Cr}$ ,  $^{62,64}\text{Ni}$ ,  $^{70}\text{Zn}$  and a  $^{208}\text{Pb}$  target are presented in Figs. 3–6. In all cases the experimental data are well reproduced, when we take into account the coupling to the low-energy surface vibrations and to the neutron transfer channels. In the calculations we used for the strength of the nuclear part of the interaction potential  $c_V$  and for the shell correction damping parameter  $\gamma$  [see Eq. (30)] the values as given in Table I. These values were obtained by fitting to the experimental data. We found that the parameter  $c_V$  is larger for the relatively light systems and close to 1 for the heavier ones. The values of the parameter  $\gamma$  increase with the element number. A similar trend was observed also in [24].

The  $2n$ -evaporation channel for the reaction  $^{50}\text{Ti} + ^{208}\text{Pb} \rightarrow ^{258}\text{Rf}^*$  is opened at a collision energy of  $\approx 184$  MeV. This energy is close to the maximum of the measured excitation function for the  $1n$  channel; see Fig. 3. The experimental data showed (see Fig. 19 in [2]) that in these relatively light systems,  $Z \leq 106$ , the  $2n$  channel does well compete with fission at excitation energies close to  $\approx 22$  MeV and is, therefore, not negligible. This is no longer the case for the heavier systems,  $Z > 106$ , where fission predominates. In our calculations, we took into account only one neutron emission for computational reasons. Therefore, the  $1n$  channel is overestimated at higher excitation energies for the relatively light systems. For that reason, we drew in Fig. 3 the calculated curves only up to values just beyond the

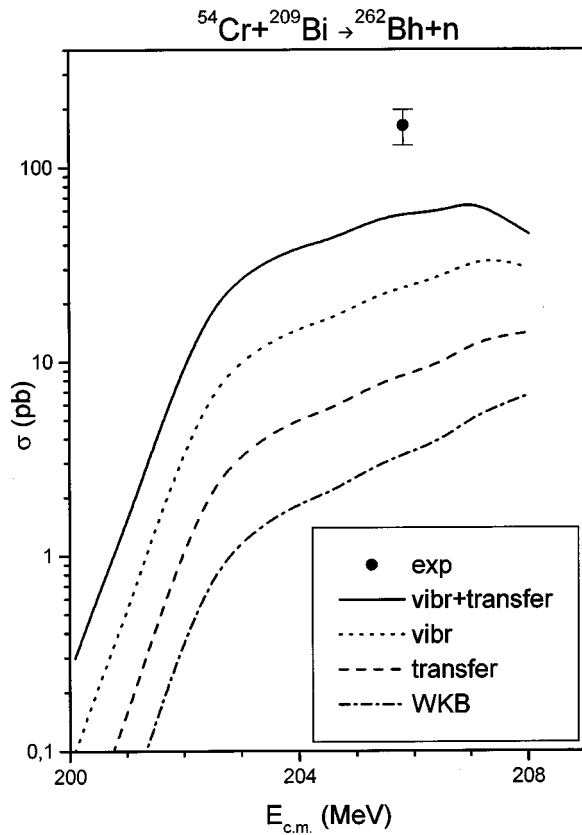


FIG. 10. Calculated excitation functions for the reaction  $^{54}\text{Cr} + ^{209}\text{Bi} \rightarrow ^{262}\text{Bh} + n$ . The inset explains the assignment of the calculations to the curves.

maximum, and similarly in Figs. 4 and 9.

The results of the calculations for reactions with the lighter and heavier target isotopes  $^{207}\text{Pb}$  and  $^{210}\text{Pb}$  are also drawn in Figs. 2 and 5–8. In Figs. 7 and 8 predictions are made for the synthesis of the so far unknown elements 114 and 116 using the reactions  $^{74,76,78}\text{Ge} + ^{207,208,210}\text{Pb}$  and  $^{80,82}\text{Se} + ^{208}\text{Pb}$ . For the values of the parameters  $c_V$  and  $\gamma$  we used the same as in the calculations for the neighboring systems; see Table I.

Using  $^{207}\text{Pb}$  or  $^{210}\text{Pb}$  as a target results in smaller cross sections as in the case of the double-magic isotope  $^{208}\text{Pb}$ . Note that in the case of reactions with  $^{207}\text{Pb}$  as target the neutron separation energy is smaller than in reactions with  $^{208}\text{Pb}$  as target, but the level density of the residue is smaller in the case of  $^{207}\text{Pb}$  (even-even residue) than for  $^{208}\text{Pb}$  (even-odd residue). Due to this the branching ratio  $\Gamma_n/\Gamma_{\text{fis}}$  is different; see also section 10.4 in [10].

The reactions using  $^{208}\text{Pb}$  and more neutron deficient projectile isotopes have in general smaller cross sections. This trend was also observed experimentally; see Fig. 5 and [2].

Especially important for the synthesis of the elements 114 and 116 using Ge and Se isotopes, respectively, is the barrier at the development to sphericity,  $B_{\text{Sph}}$ ; see Fig. 1. This barrier strongly increases with element number and reaches values of about 16 MeV for the production of the elements 114 and 116. In order to evaluate the influence of  $B_{\text{Sph}}$  on the reaction cross section, we calculated data with a reduced

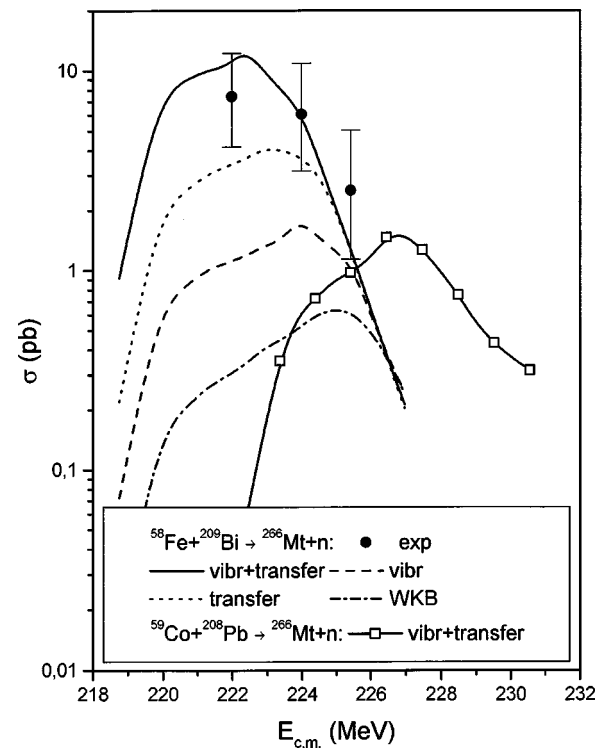


FIG. 11. Calculated excitation functions for the reactions  $^{58}\text{Fe} + ^{209}\text{Bi} \rightarrow ^{266}\text{Mt} + n$  and  $^{59}\text{Co} + ^{208}\text{Pb} \rightarrow ^{266}\text{Mt} + n$  resulting in the same compound nucleus. The inset explains the assignment of the calculations to the curves.

barrier for the reaction  $^{80,82}\text{Se} + ^{208}\text{Pb}$ . Using  $B_{\text{Sph}} = 14$  MeV results in higher cross sections by about an order of magnitude (see Fig. 8). Values of  $B_{\text{Sph}} \approx 14$  MeV are given in the literature for similar reactions [22,23].

The results obtained for the synthesis of odd elements using a  $^{209}\text{Bi}$  target are shown in Figs. 9–14. We used the same parameters  $c_V$  and  $\gamma$  as in the case of the reactions with a  $^{208}\text{Pb}$  target. Also here, the coupling to the transfer channels and to the low-energy surface vibrations is important for the relatively light systems. As for the even elements, the cross sections of the heaviest systems are dominated by the influence of the barrier  $B_{\text{Sph}}$ . The calculated cross sections are in good agreement with the available experimental data, Figs. 9–11.

The compound nuclei formed in reactions of  $^{58}\text{Fe}$ ,  $^{64}\text{Ni}$  and  $^{70}\text{Zn}$  with  $^{209}\text{Bi}$  can also be reached in reactions of  $^{59}\text{Co}$ ,  $^{65}\text{Cu}$  and  $^{71}\text{Ga}$  with  $^{208}\text{Pb}$ , respectively; see Figs. 11–13. The cross sections are larger in the reactions with  $^{209}\text{Bi}$  targets for the relatively light systems. However, in the case of the heavier systems, the cross sections using  $^{208}\text{Pb}$  or  $^{209}\text{Bi}$  are comparable. This result must be an entrance-channel effect, because the compound nucleus is the same in both cases and thus, also, the influence of the compound nucleus fission and evaporation. A similar trend is observed for the reactions  $^{78}\text{Ge} + ^{209}\text{Bi} \rightarrow ^{286}115 + n$  and  $^{75}\text{As} + ^{208}\text{Pb} \rightarrow ^{283}115 + n$ ; see Fig. 14. In recent theoretical work [16] describing the synthesis of  $^{294}119$  using the reactions  $^{86}\text{Kr} + ^{209}\text{Bi}$  and  $^{87}\text{Rb} + ^{208}\text{Pb}$  a higher cross section was obtained for the latter case.

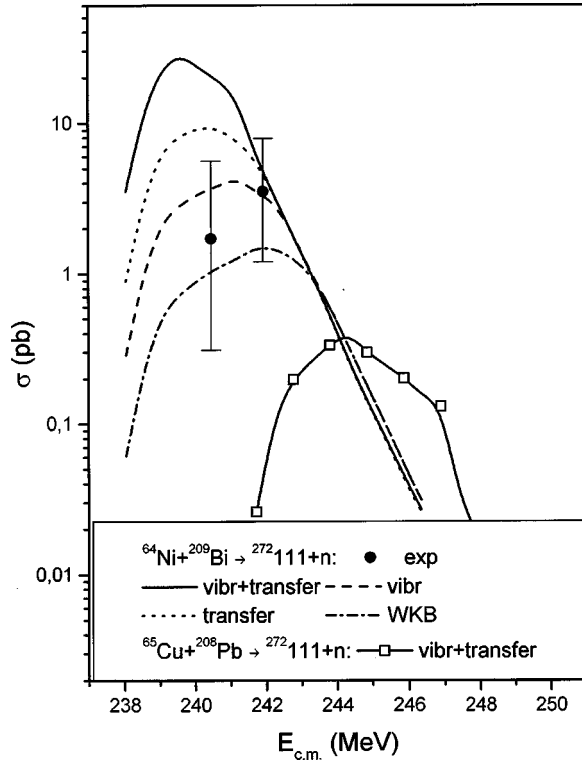


FIG. 12. Calculated excitation functions for the reactions  $^{64}\text{Ni} + ^{209}\text{Bi} \rightarrow ^{272}\text{111} + n$  and  $^{65}\text{Cu} + ^{208}\text{Pb} \rightarrow ^{272}\text{111} + n$  resulting in the same compound nucleus. The inset explains the assignment of the calculations to the curves.

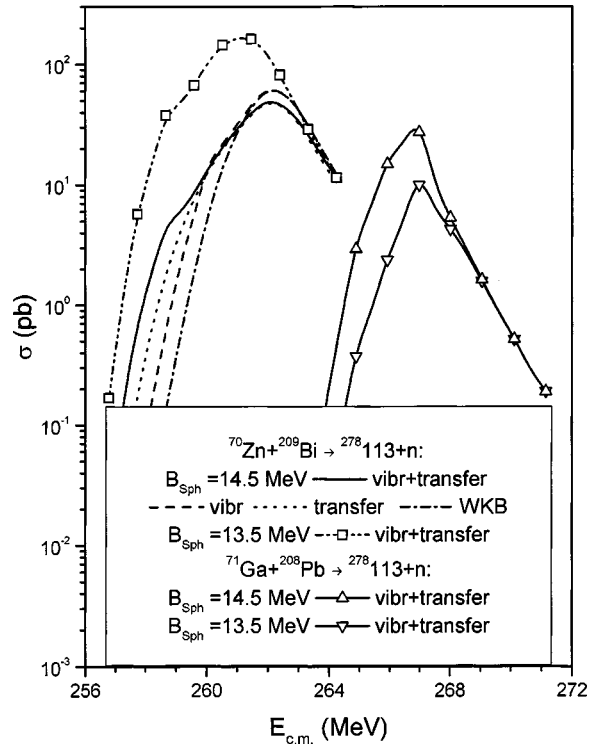


FIG. 13. Calculated excitation functions for the reactions  $^{70}\text{Zn} + ^{209}\text{Bi} \rightarrow ^{278}\text{113} + n$  and  $^{71}\text{Ga} + ^{208}\text{Pb} \rightarrow ^{278}\text{113} + n$  resulting in the same compound nucleus. The inset explains the assignment of the calculations to the curves.

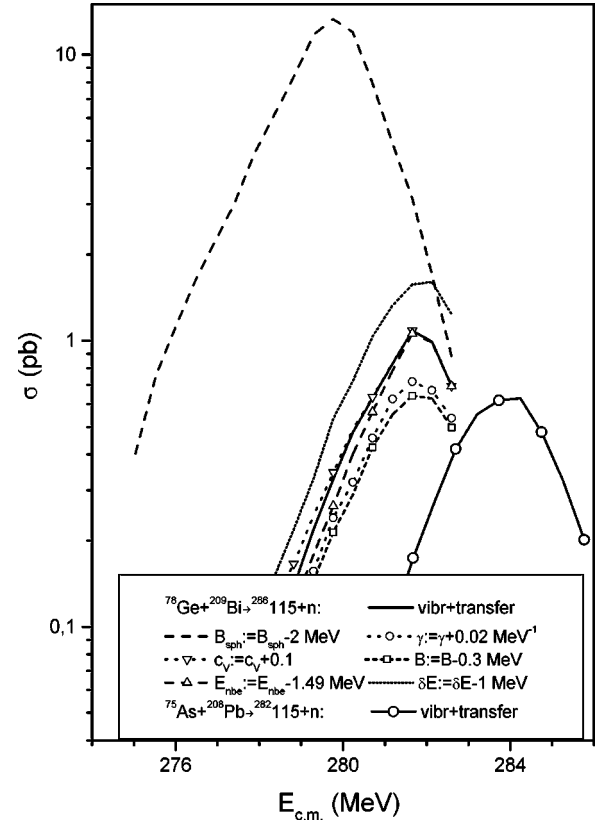


FIG. 14. Calculated excitation functions for the reactions  $^{78}\text{Ge} + ^{209}\text{Bi} \rightarrow ^{286}\text{115} + n$  and  $^{75}\text{As} + ^{208}\text{Pb} \rightarrow ^{282}\text{115} + n$ . The full lines are drawn for the nominal values of the parameters  $\gamma$  and  $c_V$ . For the influence on the cross section at the variation of the parameters see text. All curves were calculated with inclusion of the vibrations and transfer reactions.

The dependence of the cross section for the production of the SHE's on the shell-correction damping parameter  $\gamma$  [see Eq. (30)] and on the strength of the ion-ion interaction potential  $c_V$  (see Table I and related text) is shown in Fig. 14 for the reaction  $^{78}\text{Ge} + ^{209}\text{Bi} \rightarrow ^{286}\text{115} + n$ . An increase of the parameter  $c_V$  by 0.10 from the nominal value of 0.98 has only minor influence on the excitation function. Similarly small is the influence of the variation of the ground state binding energy  $E_{nbe}$ . Here we lowered the value by 1.49 MeV which is the difference of  $E_{nbe}$  between [42] and [43]. Both an increase of  $\gamma$  by  $+0.02 \text{ MeV}^{-1}$  from the nominal value of  $0.12 \text{ MeV}^{-1}$  and a decrease of the barriers  $B$  [see Eq. (32)] for compound nucleus  $B_{CN}$  and SHE  $B_{SHE}$  by  $+0.3 \text{ MeV}$  lower the cross section by about 30%. The cross section increases by about 30%, when we lower the shell-correction energy by 1 MeV for both the compound nucleus,  $\delta E_{shel}^{CN}$ , and for the ground state of the residue after neutron emission,  $\delta E_{shel}^{SHE}$ . The variation of the shell-correction energy by 1 MeV is about half of its uncertainty.

A variation of the height of the inner spherization barrier by an uncertainty value of about 2 MeV from 16 to 14 MeV increases the production cross section by one order of magnitude. As expected, also the maximum is shifted to smaller values. The use of the reaction  $^{75}\text{As} + ^{208}\text{Pb}$  for the synthesis of element 115 results only in a moderate decrease of the

cross section compared with  $^{78}\text{Ge}+^{209}\text{Bi}$ . The position of the maximum value is shifted by 2.5 MeV upwards.

## VI. CONCLUSIONS

A theoretical description of the reaction process leading to fusion of SHEs is a difficult task. The nuclei are located at the limits of stability, and the reaction process is dominated by shell structure effects in projectile, target as well as compound nucleus. In addition, shell structure is needed for the calculation of the binding energy at large deformation in order to determine the barriers for fusion,  $\bar{V}_{lk}^{i(f)}$ , formation of sphere,  $B_{\text{Sph}}$ , and fission,  $B^*$ .

The aim of our investigation was to start developing a model for the description of the cold fusion reaction. The measured cross sections and the trend to decrease by about a factor of 3 per element could be rather well reproduced. However, due to the strong dependence of the cross sections on small variations of the binding energy of the compound nucleus and the fission barrier, an extrapolation into the region of new elements is rather uncertain.

We plan to further improve our model by comparison with experimental data, which will become available in the near future. Experiments are planned for the investigation of even-even evaporation residues resulting in more accurate values for nuclear binding energies. Also, various combinations of projectile and target need to be investigated, leading to similar compound systems and thus making small, however well defined changes of the fusing system. We hope that in the case of an accurate enough reproduction of the measured cross-section values and excitation functions, it will be possible, to make more accurate predictions for the further detailed planning of experiments using various combinations of projectiles and targets for the production of SHEs.

## ACKNOWLEDGMENTS

The authors would like to thank S. Cwiok, A.V. Ignatyuk, G. Münzenberg, W. Nörenberg, A.G. Popeko, K.-H. Schmidt, and A. Sobiczewski for useful discussions; Z. Patyk also for help using the computer code WSBETA. One of us, V.Yu.D., gratefully acknowledges support from GSI.

- 
- [1] G. Münzenberg, Rep. Prog. Phys. **51**, 57 (1988).  
 [2] S. Hofmann, Rep. Prog. Phys. **61**, 373 (1998).  
 [3] G.N. Flerov, I. Zvara, G.M. Ter-Akopyan, E.D. Donets, V.A. Shchegolev, and V.L. Mikheev, Fiz. Elem. Chastits At. Yadra **22**, 931 (1991) [Sov. J. Part. Nucl. **22**, 453 (1991)].  
 [4] Yu.Ts. Oganessian, A.S. Iljinov, A.G. Demin, and S.P. Tretyakova, Nucl. Phys. **A239**, 353 (1975); Yu.Ts. Oganessian, *ibid.* **A583**, 823 (1995).  
 [5] Yu.A. Lazarev, Yu.V. Lobanov, Yu. Ts. Oganessian, V. K. Utyonkov, F. Sh. Abdullin, A.N. Polyakov, J. Rigol, I.V. Shirokovsky, Yu.S. Tsyganov, S. Iliev, V.G. Subbotin, A.M. Sukhov, G.V. Buklanov, B.N. Gikal, V.B. Kutner, A.N. Mezentsev, K. Subitic, J.F. Wild, R.W. Loughheed, and K.J. Moody, Phys. Rev. C **54**, 620 (1996); Yu.Ts. Oganessian, A.V. Yeremin, A.G. Popeko, S.L. Bogomolov, G.V. Buklanov, M.L. Chelnokov, V.I. Chepigin, B.N. Gikal, V.A. Gorshkov, G.G. Gulbekian, M.G. Itkis, A.P. Kabachenko, A.Yu. Lavrentev, O.N. Malyshev, J. Roháč, R.N. Sagaidak, S. Hofmann, S. Šaro, G. Giardina, and K. Morita, Nature (London) **400**, 242 (1999).  
 [6] S. Hofmann, F.P. Hessberger, V. Ninov, P. Ambruster, G. Münzenberg, C. Stodel, A.G. Popeko, A.V. Yeremin, S. Saro, and M. Leino, Z. Phys. A **358**, 377 (1997).  
 [7] A. Ghiorso, D. Lee, L.P. Somerville, W. Loveland, J.M. Nitschke, W. Ghiorso, G.T. Seaborg, P. Wilmarth, R. Leres, A. Wydler, M. Nurmia, K. Gregorich, R. Gaylord, T. Hamilton, N.J. Hannink, D.C. Hoffman, C. Jarzynski, C. Kacher, B. Kadkhodayan, S. Kreek, M. Lane, A. Lyon, M.A. McMahan, M. Neu, T. Sikkeland, W.J. Swiatecki, A. Türler, J.T. Walton, and S. Yashita, Nucl. Phys. **A583**, 861 (1995); A. Ghiorso, D. Lee, L.P. Somerville, W. Loveland, J.M. Nitschke, W. Ghiorso, G.T. Seaborg, P. Wilmarth, R. Leres, A. Wydler, M. Nurmia, K. Gregorich, K. Czerwinski, R. Gaylord, T. Hamilton, N.J. Hannink, D.C. Hoffman, C. Jarzynski, C. Kacher, B. Kadkhodayan, S. Kreek, M. Lane, A. Lyon, M.A. McMahan, M. Neu, T. Sikkeland, W.J. Swiatecki, A. Türler, J.T. Walton, and S. Yashita, Phys. Rev. C **51**, R2293 (1995).  
 [8] V.M. Strutinsky, Nucl. Phys. **A95**, 420 (1967); **A122**, 1 (1968).  
 [9] Yu.A. Muzychka, V.V. Pashkevich, and V.M. Strutinsky, Yad. Fiz. **8**, 716 (1968) [Sov. J. Nucl. Phys. **8**, 417 (1969)].  
 [10] R. Vandenbosch and J.R. Huizenga, *Nuclear Fission* (Academic Press, New York, London, 1973).  
 [11] P. Möller and J.R. Nix, J. Phys. G **20**, 1681 (1994).  
 [12] G.G. Adamian, N.V. Antonenko, W. Scheid, and V.V. Volkov, Nucl. Phys. **A633**, 409 (1998).  
 [13] V.V. Volkov, G.G. Adamian, N.V. Antonenko, E.A. Cherepanov, and A.K. Nasirov, Nuovo Cimento A **110**, 1127 (1998).  
 [14] Y. Abe, Y. Arimoto, T. Wada, and M. Ohta, J. Phys. G **23**, 1275 (1997).  
 [15] F.A. Ivanyuk, G.I. Kosenko, Yu. Ts. Oganessian, and V.V. Pashkevich, in *Proceedings of the Tours Symposium on Nuclear Physics 3*, edited by M. Arnould, M. Lewitowicz, Yu. Ts. Oganessian, M. Ohta, H. Utsunomiya, and T. Wada, AIP Conf. Proc. No. 425 (AIP, New York, 1998), p. 75.  
 [16] R. Smolanczuk, Phys. Rev. C **59**, 2634 (1999).  
 [17] R. Smolanczuk, J. Skalski, and A. Sobiczewski, Phys. Rev. C **52**, 1871 (1995).  
 [18] R. Smolanczuk, Phys. Rev. C **56**, 812 (1997); Phys. Rev. Lett. **83**, 4705 (1999); Phys. Rev. C **60**, 021301 (1999); **61**, 011601(R) (2000).  
 [19] S. Cwiok, V.V. Pashkevich, J. Dudek, and W. Nazarewicz, Nucl. Phys. **A410**, 254 (1983).  
 [20] S. Cwiok and A. Sobiczewski, Z. Phys. A **342**, 203 (1992).  
 [21] S. Cwiok, S. Hofmann, and W. Nazarewicz, Nucl. Phys. **A573**, 356 (1994).  
 [22] P. Möller, J.R. Nix, P. Ambruster, S. Hofmann, and G. Mün-

- zenberg, Z. Phys. A **359**, 251 (1997); (private communications).
- [23] P. Möller and J.R. Nix, Los Alamos National Laboratory Report No. LA-UR-97-3580.
- [24] Z. Lojewski, V.V. Pashkevich, and S. Cwiok, Nucl. Phys. **A436**, 499 (1985).
- [25] P. Möller, J.R. Nix, and W.J. Swiatecki, Nucl. Phys. **A492**, 349 (1989).
- [26] M. Diebel, K. Albrecht, and R.W. Hasse, Nucl. Phys. **A355**, 66 (1981).
- [27] K.-H. Schmidt and W. Morawek, Rep. Prog. Phys. **54**, 949 (1991).
- [28] R. Bass, *Nuclear Reaction with Heavy Ions* (Springer-Verlag, Berlin, 1980).
- [29] M. Beckerman, Phys. Rep. **129**, 145 (1985); Rep. Prog. Phys. **51**, 1047 (1988).
- [30] A.B. Balantekin and N. Takigawa, Rev. Mod. Phys. **70**, 77 (1998).
- [31] V.M. Shilov and A.V. Tarakanov, Yad. Fiz. **56**, 55 (1993) [Phys. At. Nucl. **56**, 741 (1993)].
- [32] C.H. Dasso and S. Landowne, Comput. Phys. Commun. **46**, 187 (1987).
- [33] V.Yu. Denisov, Yad. Fiz. **62**, 1431 (1999) [Phys. At. Nucl. **62**, 1349 (1999)]; Eur. Phys. J. A (to be published).
- [34] L. Corradi, in *Proceedings of the Workshop on Heavy Ion Fusion: Exploring the Variety of Nuclear Properties*, Padova, Italy, 1994, edited by A.M. Stefanini *et al.* (World Scientific, Singapore, 1994), p. 34.
- [35] W. von Oertzen, Report No. HMI-B556 (1998).
- [36] K.E. Rehm, Annu. Rev. Nucl. Part. Sci. **41**, 429 (1991).
- [37] V.Yu. Denisov, Yad. Fiz. **54**, 1556 (1991) [Sov. J. Nucl. Phys. **54**, 952 (1991)]; V.Yu. Denisov and G. Royer, J. Phys. G **20**, L43 (1994); V.Yu. Denisov and G. Royer, Yad. Fiz. **58**, 448 (1995) [Phys. At. Nucl. **58**, 397 (1995)]; V.Yu. Denisov and S.V. Reshitko, *ibid.* **59**, 81 (1996) [*ibid.* **59**, 72 (1996)].
- [38] L.D. Landau and E.M. Lifshits, *Quantum Mechanics. Nonrelativistic Theory* (Pergamon Press, Oxford, 1977).
- [39] D.L. Hill and J.A. Wheeler, Phys. Rev. **89**, 1102 (1953).
- [40] H.J. Krappe, J.R. Nix, and A.J. Sierk, Phys. Rev. C **20**, 992 (1979).
- [41] G. Audi and A.H. Wapstra, Nucl. Phys. **A595**, 409 (1995).
- [42] W.D. Myers and W.J. Swiatecki, Nucl. Phys. **A601**, 141 (1996).
- [43] P. Möller, J.R. Nix, W.D. Myers, and W.J. Swiatecki, At. Data Nucl. Data Tables **59**, 185 (1995).
- [44] G. Royer, R.K. Gupta, and V. Denisov, Nucl. Phys. **A632**, 275 (1998).
- [45] S. Cwiok, J. Dudek, W. Nazarewicz, J. Skalski, and T. Werner, Comput. Phys. Commun. **46**, 379 (1987).
- [46] H.J. Lipkin, Ann. Phys. (N.Y.) **9**, 272 (1960); Y. Nogami, Phys. Rev. **134**, B313 (1964).
- [47] P. Möller, and J.R. Nix, Nucl. Phys. **A361**, 117 (1981).
- [48] K.A. Snover, Annu. Rev. Nucl. Part. Sci. **36**, 545 (1986).
- [49] F.D. Becchetti and G.W. Greenlees, Phys. Rev. **182**, 1190 (1969).
- [50] A. Bohr and B.R. Mottelson, *Nuclear Structure* (Benjamin, Reading, MA, 1975).
- [51] G.D. Adeev and P.A. Cherdantsev, Yad. Fiz. **18**, 741 (1974) [Sov. J. Nucl. Phys. **18**, 381 (1974)].
- [52] A.V. Ignatyuk, K.K. Istekov, and G.N. Smirenkin, Yad. Fiz. **29**, 875 (1979) [Sov. J. Nucl. Phys. **29**, 450 (1979)].
- [53] A.V. Ignatyuk, M.G. Itkis, and S.I. Mulgin, Fiz. Elem. Chastits At. Yadra **16**, 709 (1985) [Sov. J. Part. Nucl. **16**, 307 (1985)].
- [54] A.V. Ignatyuk, G.N. Smirenkin, and A.S. Tishin, Yad. Fiz. **21**, 485 (1975) [Sov. J. Nucl. Phys. **21**, 255 (1975)].
- [55] K.-H. Schmidt, H. Delagrange, J.P. Dufour, N. Carjan, and A. Fleury, Z. Phys. A **308**, 215 (1982).
- [56] A.S. Jensen and J. Damgaard, Nucl. Phys. **A203**, 578 (1973).
- [57] S. Raman, C.W. Nestor, S. Kahane, and K.H. Bhatt, At. Data Nucl. Data Tables **42**, 1 (1989).
- [58] R.H. Spear, At. Data Nucl. Data Tables **42**, 55 (1989).
- [59] C.M. Baglin, Nucl. Data Sheets **69**, 733 (1993).
- [60] M.R. Bhat, Nucl. Data Sheets **69**, 209 (1993).
- [61] S. Rab, Nucl. Data Sheets **63**, 1 (1991).
- [62] M.R. Bhat, Nucl. Data Sheets **68**, 579 (1993); M.R. Bhat, and D.E. Alburger, *ibid.* **53**, 1 (1988).
- [63] A.R. Farhan and S. Rab, Nucl. Data Sheets **60**, 735 (1988).
- [64] J. Alster, Phys. Rev. **141**, 1138 (1966).
- [65] M.J. Martin, Nucl. Data Sheets **63**, 723 (1991).